2011

A comprehensive study of dust formation and evolution in core collape supernovae

Jennifer Erin Andrews
Louisiana State University and Agricultural and Mechanical College, jandrews@phys.lsu.edu

A COMPREHENSIVE STUDY OF DUST FORMATION AND EVOLUTION IN CORE COLLAPSE SUPERNOVAE

A Dissertation

Submitted to the Graduate Faculty of
the Louisiana State University and
Agricultural and Mechanical College
in partial fulfillment of the
requirements for the degree of
Doctor of Philosophy

in

The Department of Physics and Astronomy

by
Jennifer Andrews
B.S., College of Charleston, 2005
M.S., Louisiana State University, 2009
May, 2011

To Jeff and my parents, for all their love and support the last few years.

Acknowledgments

This dissertation would not be possible without the love, support, and guidance of many friends, family members and mentors. First I would like to thank Geoffrey Clayton for providing me with the tools and pushing me to be the best astronomer that I possibly could be. He has had extreme patience, putting up with me good days and bad. In the same manner, thanks is extended to Ben Sugerman for being a wonderful life coach and for answering any and all questions I sent his way, big or small. I would also like to thank Margaret Meixner for her mentorship, and the 30-odd letters of reference she provided, along with Geoff and Ben, which helped me not only get a job but actually have a choice in one. To the rest of the SEEDS team Joe Gallagher, Doug Welch, Mike Barlow, Roger Wesson, Joanna Fabbri, Masaaki Otsaku, thank you for providing expertise and assistance the last few years. I would also like to thank my fellow graduate students Ashley Pagnotta, Brent Budden, Bill Plick, Sean Huver, and Ryan Glasser for making graduate school more than just a place to get an education, but a place to find a family away from home. To my non-physics friends Liz Cooke, Kristin Budden, Jason Hessick, Sara DeRosa, and others, thanks for putting up with all of us the past few years, and more importantly thank you for your friendship. And to the rest of Team Clayton, including Bill, Jan, and Nutsinee, thanks for making coming into the office a little more enjoyable and entertaining at times!

I would also like to thank my parents David and Wanda Andrews, and my grandparents Earl and Mary Andrews, who never for a second let me believe there was anything I couldn't do, and who have always wanted me to be successful in whatever path I chose in life. Also, a special thanks to Aidan Brooks for giving me encouragement on those days where it seemed all was lost. And last but certainly not least, I would like to thank my fiancee Jeff Kissel, with whom I embarked on this graduate school journey, and without whom these past 5 years would have been a million times more difficult. Through his love and support, and most importantly his patience, he has made it possible for me to make it to this important point in my life. I love you Jeff.

Table of Contents

List of Tables

List of Figures

Abstract

Detection of large amounts of dust in high redshift galaxies suggests that core collapse supernovae (CCSNe) may play a critical role in the dust budget of galaxies in the early universe, when galaxies are only a few hundred million years old. At an age of only 1Gyr, asymptotic giant branch (AGB) stars may not have had the time to become significant dust contributors, leaving CCSNe as an alternative explanation since they quickly evolve and return their material to the surrounding interstellar medium. For the past three years, I have been observing the CCSNe 2007it and 2007od with Gemini, Hubble Space Telescope, and Spitzer Space Telescope in the optical and infrared to look for indicators of dust formation, which appear within the first few years after explosion. The data sets contain large temporal and wavelength coverage, and have led to some unusual and interesting results. In both cases there is evidence for interaction with surrounding circumstellar material (CSM), although neither was classified as a Type IIn. SN 2007it was found to be oxygen rich with a ^{56}Ni mass quite large for a Type IIP, while SN 2007od is oxygen poor with a very low, over two orders of magnitude less, ^{56}Ni mass. Scattered light echoes also seem to be present in both SNe. An estimated $\sim 10^{-4}$ $M_{\odot}$ of new dust has formed in each SN, consistent with other CCSNe, but still significantly less than needed to account for the amount of dust seen at high redshift. I will discuss these results and their implications for SNe as major dust contributors in the universe.

1. Introduction

1.1 Dust in Primordial Galaxies

The study of the role of core collapse supernovae (CCSNe) as major contributors to dust production in the Universe has grown dramatically over the last few years. This is due to the discovery of high redshift galaxies containing massive amounts of dust (Bertoldi et al., 2003). The presence of this dust in at least three galaxies with z > 6, and a handful of galaxies with z > 5 (Michałowski et al., 2010a) where very little was expected challenges our understanding of major dust contributors in the Universe. Observations of these galaxies indicate that they contain at least $10^8 M_\odot$ of cool dust (Bertoldi et al., 2003). The origin of this dust is still under much contention, whether it be from quick, explosive processes such as CCSNe or from slow, quiescent processes such as from the atmospheres of asymptotic giant branch (AGB) stars (Dwek et al., 2007). CCSNe, which can quickly return their material back into the surrounding ISM, are attractive potential producers of dust seen at high-z. It is important to understand the underlying mechanisms that create and destroy dust in the interstellar medium (ISM) in order to correctly interpret both the properties of galaxies, and processes occurring within them.

In the current epoch, the stellar sources of dust in the Milky Way can be traced to a few different types of objects. Evolved stars, such as red giants and supergiants and grains from the winds of carbon stars constitute roughly 50% of the dust added into the ISM per year, with planetary nebulae contributing another 40% (although Gehrz (1989) has published a number closer to 1%). CCSNe produce about 5% of the dust in the Milky Way, while Wolf-Rayet stars, novae and T-Tauri stars each contribute less than 1% of the dust in the galaxy (Gehrz, 1989; Draine, 2009). The dust produced by stellar sources is still only less than 5% of the dust produced in the ISM. It is believed that most of the dust mass formed in the ISM may actually condense out of the cold gas onto pre-existing dust grain seeds in a process known as depletion (Draine, 2009).

Up to 1 $M_\odot$ of dust per SN would be needed to account for the dust seen at high-z according to the work of Todini & Ferrara (2001) and Nozawa et al. (2003). Some studies of nearby SNe have been undertaken in order to estimate dust masses, but at the most only 10^{-2} $M_\odot$ of newly formed dust has been detected (Sugerman et al., 2006), with the average newly formed dust masses being 10^{-3}-10^{-4} $M_\odot$ (Elmhamdi et al., 2003b; Meikle et al., 2007; Kotak et al., 2009, for example). Low mass stars take much longer to evolve into the dust producing AGB phase, and may not have had enough time to evolve in galaxies less than 1 Gyr old (Dwek et al., 2007; Michałowski et al., 2010b). If star formation began at z=10, then by z=6.4 the oldest stars are only 400 Myr old. Recent papers by Valiante et al. (2009), Sloan et al. (2009), and Dwek & Cherchneff (2010) suggest AGB stars may be significant dust contributors as early as ∼150-500 Myr. Michałowski et al. (2010b) find that in six submillimeter galaxies with z > 4, the dust content of three can be explained by AGB stars, while the remaining three can only be explained by CCSNe. Finally, Draine (2009) postulates that as in the Milky Way, most of the dust in high-z galaxies forms out of the cold gas of the ISM on grains produced by stellar sources. For these grains to form so early, they do need fast evolving supernovae to produce both the metals that compose the grains, and dust to provide the initial surface area for larger grains to form through depletion. Many questions still remain on the source of high-z dust.

Pre-existing grains in the ISM, be it from AGB stars, SNe, or grain growth, once subjected to a nearby supernovae explosion will have a difficult time withstanding the high velocities ($>$ 5000 km s^{-1}) and high temperatures ($>$ 2000 K) created by the supernova shock. This is why at the current epoch, supernovae are actually net destroyers of dust. Although, in the first few billion years after galaxy formation, the amount of dust produced from supernovae was significantly greater than the dust destroyed by supernova shocks, which expanded into an essentially dust free ISM, making them important contributors to dust in the early universe (Dwek, 1998). We cannot observe SNe in these high-z galaxies, but we can observe nearby ones in order to understand the current role of CCSNe in dust production. This increased understanding of dust formation from massive stars can then be applied to understanding the presence of large amounts of dust in primordial galaxies seen at high redshift.

1.2 Supernova Classification

Supernovae are classified into either Type I or Type II based upon their optical spectra. The absence of hydrogen is a signature of a Type I SN, while prominent hydrogen lines (particularly Hα at 6563 Å) defines a Type II SN. Type II SNe are sub-divided based on light curve evolution, and Type IIP (P is for plateau) SNe show an extended plateau phase of almost constant luminosity lasting $\sim$ 70-110 days due to radiative cooling of the shock-heated hydrogen envelope as well as energy released from hydrogen recombination (Grassberg et al., 1971). If the lightcurve falls off linearly with time, it is classified as a Type IIL (L is for linear). See Figure 1.1 for a comparison. When the age of the Type IIP and Type IIL SNe reach about 150 days, the light curves begin to look identical, both in shape and flux level (Filippenko 1997), due to the radioactive decay of ^{56}Co, with the luminosity being constrained by the amount of ejected ^{56}Ni (Weaver & Woosley, 1980). Type IIP SNe make up almost 60% of CCSNe, while Type IIL are only about 2% (Smartt et al., 2009). The progenitors of the Type II subclass are thought to be red supergiants (RSG) with masses in the range of 8-25 M$_\odot$ (Eldridge & Tout, 2004; Heger et al., 2003) that steadily lose their atmospheres with winds of 10-15 km s^{-1}. Type IIP SNe would then come from progenitors that have only lost a small fraction of their hydrogen envelope, while Type IIL SNe progenitors would have lost a larger fraction more, but not as much as Type Ib/c (discussed below). Recently, a comprehensive analysis by Smartt et al. (2009) did not find any evidence for progenitors above 17 M$_\odot$, which may indicate a disconnect between theory and observation since theoretical models of CCSNe progenitors, such as those listed in Maguire et al. (2010), have estimated progenitor masses of up to 29 M$_\odot$. Therefore the search is ongoing for detection of more massive progenitors.

The spectra of Type II SNe start out at maximum with a nearly continuous spectra, with only weak hydrogen and helium lines visible with P Cygni profiles. These lines are very broad due to the high velocity of the ejecta. During this time the temperature is also rapidly falling as the ejecta expands and the density falls. For Type IIP, between days 40-100 after maximum, not much changes as the temperature remains constant and the energy deposited by the shock is released into the hydrogen ejecta. This is the plateau phase where the medium is not transparent for electrons, allowing the excited hydrogen atoms to recombine and reheat the ejecta. For Type IIL during this time Hα emission is greatly increasing, while Hβ, Na I, and Fe II are becoming stronger as well. At around day 100, lines of Ca II, Na I, Fe II, Ti II and Sc II can be seen in the spectra of both types of Type II SNe, and a few weeks later strong [O I] $\lambda\lambda$ 6300, 6364 emission lines are visible, this is the start of the nebular phase of the SNe. During the nebular phase, the expanding ejecta has finally cooled

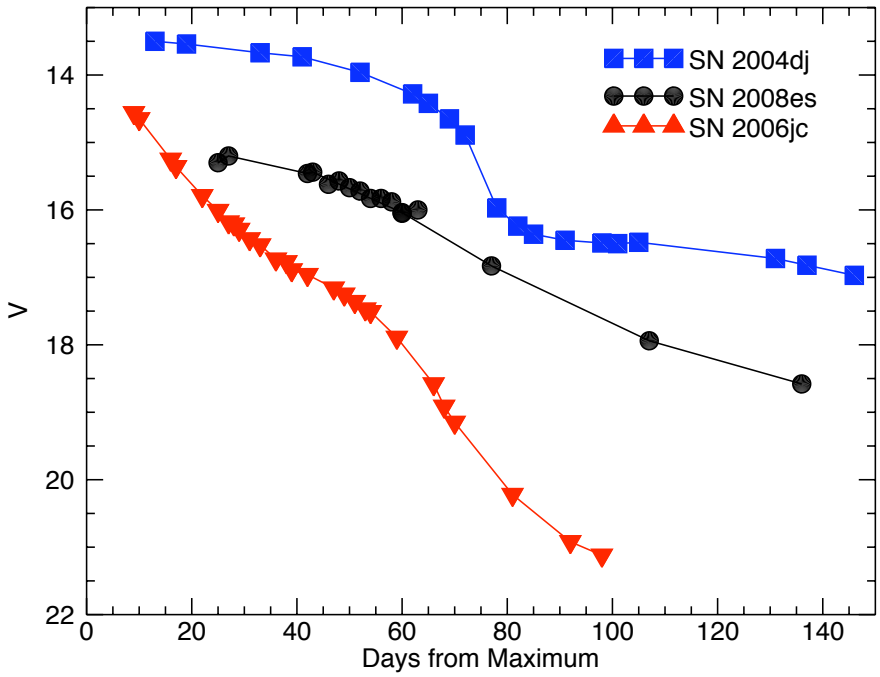

Figure 1.1: Examples of the V band light curves of a Type IIP (SN 2004dj), a Type IIL (SN 2008es), and a Type Ib/c (SN 2006jc). Data are from Miller et al. (2009); Anupama et al. (2009); Zhang et al. (2006). Data points for SN 2008es have been shifted up 2.5 magnitudes, and data for SN 2004dj down 1.5 magnitudes. The steepness of the SN 2006jc lightcurve after day 60 is likely due to early dust formation.

to temperatures under 2000K. The continuum has visibly faded, leaving strong Hα, calcium, and oxygen lines, along with some weaker metal emission lines (Filippenko, 1997). Figure 1.2 shows an example of a Type II spectrum.

At early times, some Type II SNe spectra show a narrow peak sitting atop a broad base in the hydrogen and helium lines, with no P Cygni component (Figure 1.2). These narrow lines give them the classification Type IIn. Normal Type II RSG progenitors only lose about 10^{-6} to 10^{-5} $M_\odot$ yr^{-1} (Chevalier et al., 2006), which is usually too tenuous to show any circumstellar medium (CSM) interaction. The progenitors of Type IIn SNe on the other hand lose orders of magnitude more material, 10^{-2} to 10^{-1} $M_\odot$ yr^{-1} (Kiewe et al., 2010), which result in narrow ($\sim$ 100 km s^{-1}) emission lines in their spectra due to ionization of the pre-existing CSM which has been excited by the initial flash of the supernova. Due to interaction with circumstellar debris surrounding them, these SNe do not decline in brightness very quickly at early times, and usually can be detected in both the x-ray and radio regimes. Throughout their evolution there are strong emission lines, but little to no absorption lines present. Type IIn supernovae can have either a linear or plateau like light curve, and are about 4% of the total CCSNe population.

Finally, Type Ib/c SNe occur from the core collapse of massive stars that have expelled all

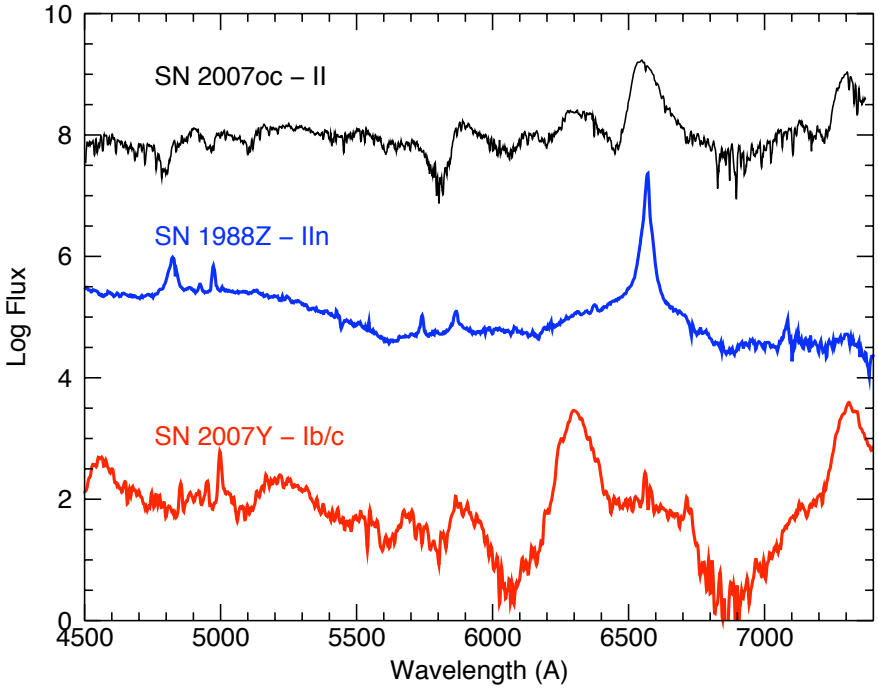

Figure 1.2: Example optical spectra for a Type II (SN 2007oc), Type IIn (SN 1988Z), and Type Ib/c (SN 2007Y) SN. Data are from Turatto et al. (1993b) and Stritzinger et al. (2009).

of their hydrogen envelopes. There is some speculation as to whether there are distinctions between Ib and Ic, with the belief that SN Ib still contain their helium envelope and SN Ic have lost both the hydrogen and helium envelope. An example spectrum of a Type Ib/c SN is shown in Figure 1.2. Due to their lack of hydrogen envelope, Type Ib/c SNe light curves resemble Type IIL SNe (Figure 1.1). The likely progenitors of these SNe are massive Wolf Rayet (WR) stars that have shed some if not all of their hydrogen envelope, or a binary system in which Roche lobe overflow has occurred and the hydrogen envelopes have been stripped. These objects are about 30% of CCSNe (Smartt et al., 2009).

1.3 Dust Formation Signatures

The mechanism and efficiency of dust condensation in CCSNe ejecta is not well understood, largely due to the lack of observational data. Signatures of condensing dust have been observed approximately 1-2 yr after the initial explosion in a very few SNe. This is when the expanding ejecta has entered the nebular phase and has cooled to temperatures below 1800K (the temperature at which amorphous carbon dust can condense). At these temperatures, the gas becomes supersaturated, and nucleation creates large clusters (Bianchi & Schneider, 2007). As dust condenses in the expanding SN ejecta, it can be detected by: (1) A sudden decrease in continuum brightness in the visible due to increased dust extinction, (2)

the development of an infrared excess in the SN light curve arising from dust grains absorbing high-energy photons and re-emitting them in the infrared, and (3) the development of asymmetric, blue-shifted emission-line profiles caused by dust in the ejecta preferentially extinguishing redshifted emission. All three of these signatures were seen for the first time in SN 1987A (Lucy et al., 1989; Wooden et al., 1993), then in SN 2003gd (Sugerman et al., 2006; Meikle et al., 2007), and also SN 2004et (Sahu et al., 2006; Kotak et al., 2009).

1.3.1 Decrease in Continuum Brightness in Visible

Up until a few hundred days post-explosion, the visible light curve of a CCSNe should follow a decline similar to those seen in Figure 1.1. The expanding SN ejecta eventually becomes optically thin at around two hundred days, and becomes dominated by the decay of ^{56}Co. This creates a very linear decline, with a slope equal to the half-life of ^{56}Co (see Figure 1.3). Models of bolometric light curves use this radioactive decay (dotted line in Figure 1.3) to estimate the brightness of a CCSNe at any given time (Pinto et al., 1988). If the observed lightcurve shows a deviation from the predicted luminosity, one can conclude that there could be material either obscuring or scattering the light from the SN. If there is a noticeable decrease in brightness of the visible lightcurve, it is likely that the formation of dust grains has occurred in the ejecta of the SN and is obscuring a fraction of the light. If, on the other hand, the lightcurve of the SN flattens (especially at late times) and remains brighter than predicted from the slope of ^{56}Co decay, this could indicate the presence nearby circumstellar material (CSM) or interstellar material (ISM) that is creating a scattered light echo from the SN light. This was seen, for example, in SN 2002hh (Welch et al. 2005). If the object happens to be close enough or the material far enough away from the SN, these light echoes can be resolved with telescopes such as HST. This will be discussed in more detail in Chapters 3 and 4.

1.3.2 Infrared Excess

At the same time that there is a significant drop in the continuum brightness in the visible, there should be a corresponding brightening in the infrared (see Figure 1.4). This happens because the higher energy photons (optical and UV) that are being emitted through the ^{56}Co decay are being absorbed by the dust particles and being re-emitted in the infrared (Dwek et al., 2007). Unfortunately the IR signature is complicated by the fact that it includes heating of pre-existing circumstellar dust. CCSNe have massive-star progenitors which have winds that formed circumstellar shells. These shells can then themselves reemit high energy photons in the infrared, making it difficult to distinguish between newly formed dust and pre-existing dust. For this reason it is important to observe SN often and over long time periods in the IR to create a baseline to compare any deviations in IR luminosity in order to detect dust formation.

1.3.3 Asymmetric, Blue-Shifted Emission-line Profiles

The final indicator for dust formation is the attenuation of the red wings of the optical emission lines of the ejecta of the supernova. See Figure 1.6. As in the case of the decline in the visible, the dust particles are absorbing the visible photons and re-emitting them in the infrared. The broad ejecta lines of the SN are created from the fast moving ($\sim$ 7000 km s^{-1}) ejected gas. If a spherically symmetric model is assumed for the SN, where the

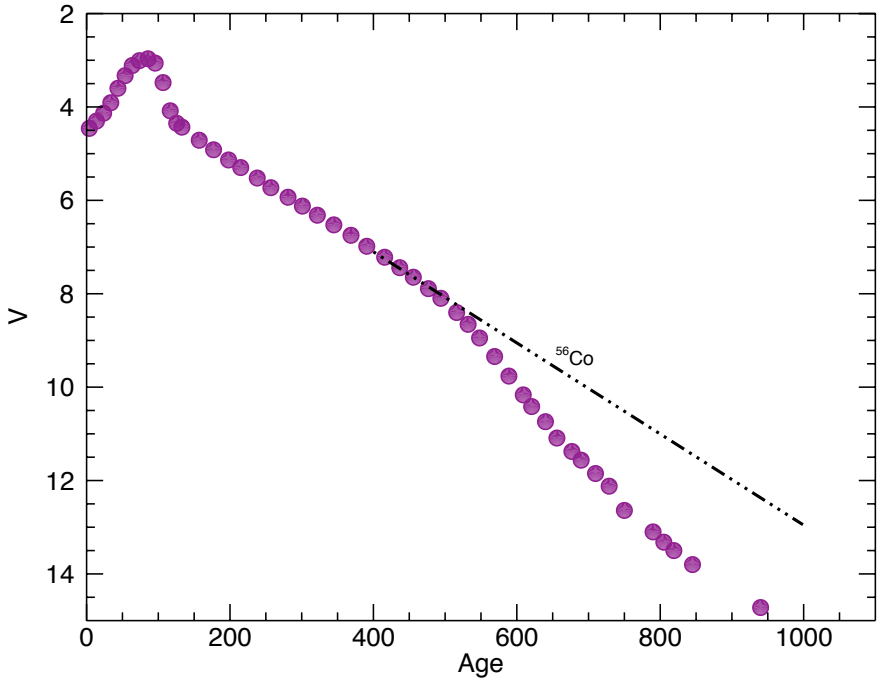

Figure 1.3: The V-band lightcurve of SN 1987A. Notice the deviation from ^{56}Co decay after day 500. The data come from Caldwell et al. (1993, and references therein).

dust has formed inside of the ejecta front, spectra taken at this time will be much stronger in the blue side than the red due to the fact there is more dust between the red side and the observer, and more chances for absorption of the visible continuum and remission in the infrared. This is illustrated in Figure 1.5. This translates into a decrease of the red wings of the emission-line profiles as the optical light from the red side gets absorbed by the dust, giving the appearance of asymmetric and blue shifted lines (Dwek et al., 2007). Unfortunately detection of these asymmetries requires very high signal-to-noise and spectral resolution some 1-2 years after explosion when the SN has dimmed dramatically, so large ground based or space based telescopes are needed. This has created a lack of extensive high resolution late-time optical spectra until recently.

1.4 Dust in SN 1987A

Supernova 1987A was a peculiar Type II SN discovered in the Large Magellanic Cloud (LMC) on February 24, 1987, and was the first supernova visible to the naked-eye since Kepler's supernova in 1604. Due to its proximity and brightness (V magnitude $\sim$3), SN 1987A has been the most well studied and documented SN to date. The light curve and spectra suggest that it mostly resembles a Type IIP SN, although it had some unusual characteristics. It is a unique supernova in that its progenitor was actually a blue supergiant, rather than a

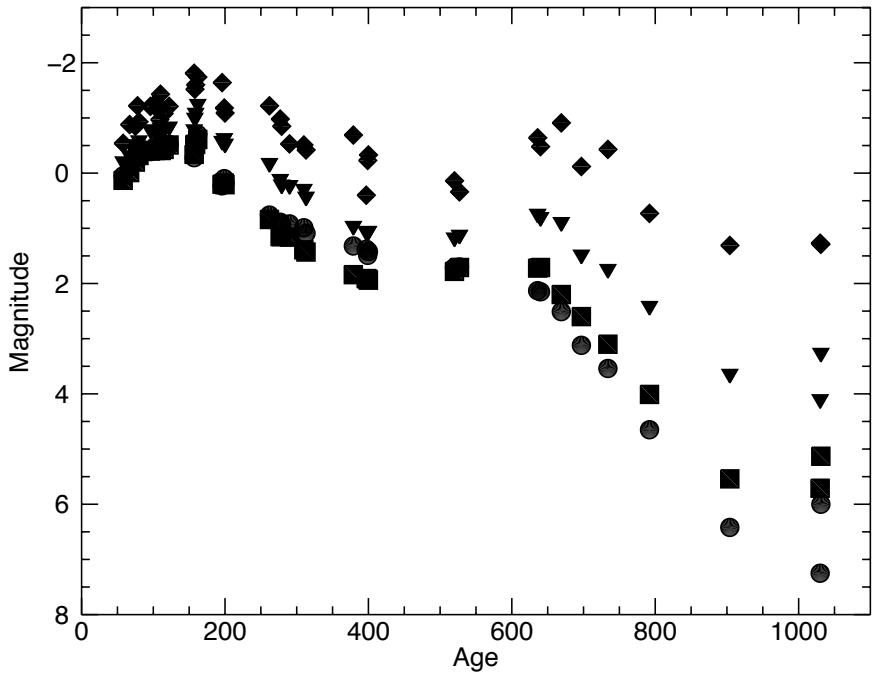

Figure 1.4: Lightcurves of SN 1987A in the N1(circles), N2 (squares), N3 (triangles), and Q0 (diamonds) broadband IR filters. The central wavelengths are 8.38, 9.69, 12.89, and 18.56 μm respectively. Notice the increase in IR luminosity after day 500, which is due to the formation of new dust grains which absorbs UV/optical photons and re-emitt them in the IR. Data are from Bouchet et al. (1989) and Bouchet & Danziger (1993).

red supergiant which is thought to be the normal progenitor of Type II SNe (Woosley et al., 1987). It was also the first CCSNe to show signs of newly formed dust in the ejecta. The spectral evolution of SN 1987A was very similar to a normal Type IIP up until day 530 when Lucy et al. (1989) reported the blueshift of several emission lines. Figure 1.6 shows the spectral evolution of the [O I] $\lambda\lambda$ 6300,6364 Å from April 1988 to April 1989 when the dust formation and the corresponding noticeable blue shifts have occurred. Suntzeff et al. (1991) also discovered that around day 500, there was a sudden increase in the mid-infrared (10 and 20 μm) flux, with a corresponding fast decline in the V band light curve. Figure 1.4 shows the mid-IR evolution and Figure 1.3 shows the evolution of the V band lightcurve of SN 1987A. These combined observational data gave us the first conclusive evidence of dust forming in the ejecta of a CCSNe.

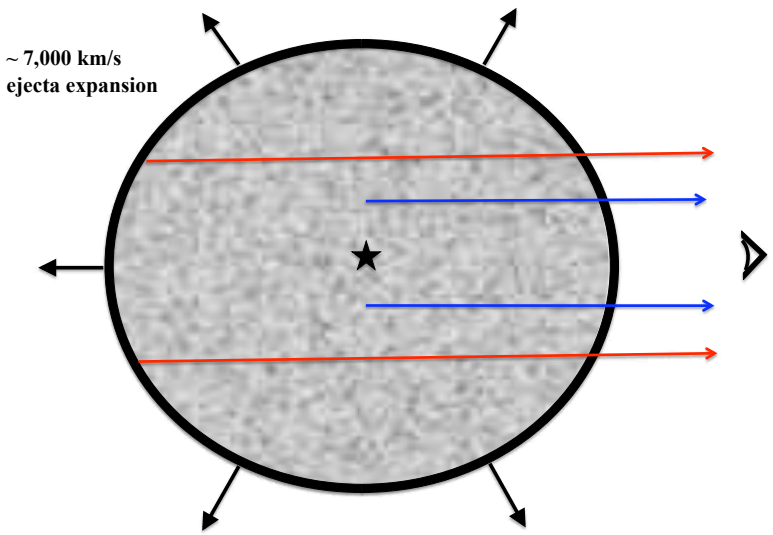

Figure 1.5: Cartoon of the geometry of a spherical SN ejecta. If dust is formed symmetrically around the explosion site, emission lines will be attenuated more on the red side due to the increased extinction through the ejecta which is proportional to the path length.

1.5 Dust from CSM Interaction

A few CCSNe have shown evidence for early dust formation, between 50-250 days. SN 1998S formed dust sometime between days 140-268 (Leonard et al., 2000), while SN 2006jc showed dust formation signatures between days 50-75 (Mattila et al., 2008; Smith et al., 2008). The SNe which show signs of early dust formation all have ejecta interacting with a dense, nearby circumstellar medium. The dust may form in a cool dense shell (CDS) between the forward and reverse shocks (Chevalier & Fransson, 1994; Pozzo et al., 2004). The formation of dust in the CDS allows for an additional avenue of dust formation not available in normal Type II SNe. The capability to form dust both within the SN ejecta and in the CDS suggests that these interacting systems have potential for forming dust in greater quantities than normal Type II SNe, although to date they have produced dust amounts comparable to normal Type II SNe.

Interaction with surrounding CSM or ISM seems to be inevitable for CCSNe, since the progenitors are massive stars that suffer significant mass loss. Signs of this interaction can be seen within the first few days of the explosion in the form of narrow emission lines in Type IIn SNe, when a SN explodes either during or shortly after a significant mass loss event of the progenitor. More recently, with the use of large ground-based and space telescopes, we have been able to follow CCSNe years after the explosion and are finding evidence of light echoes of the SN in the surrounding ISM (and sometimes CSM) material, where the early time light pulse of the SN is reflected in the visble or re-emitted in the IR. This phenomenon

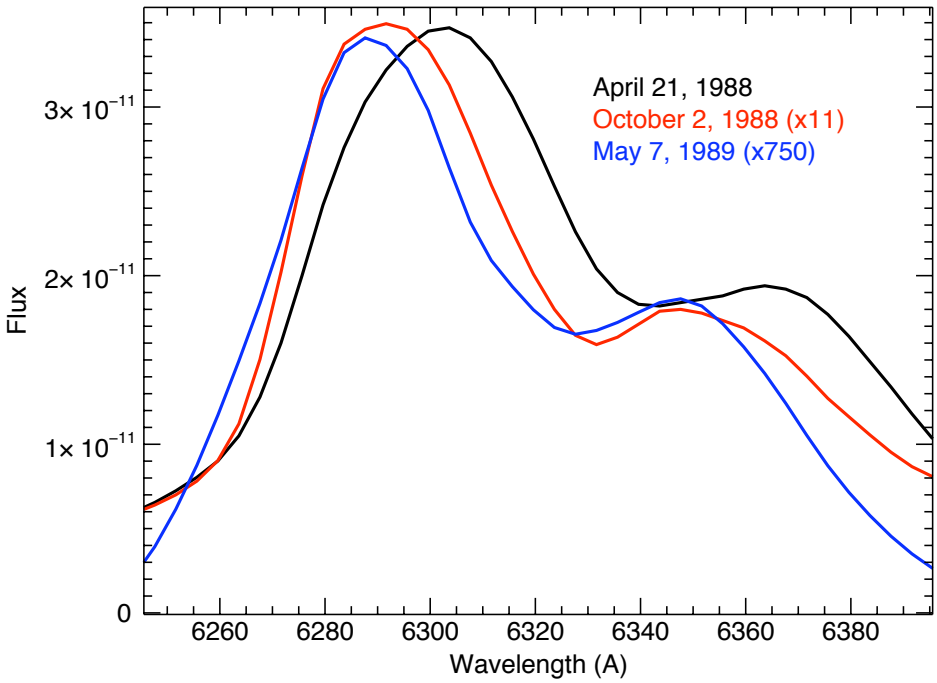

Figure 1.6: Spectral evolution of SN 1987A for April 21, 1988 (black), October 2, 1988 (red), and April 19, 1989 (blue). Data were downloaded from the Suspect Database, and are courtesy of Pun et al. (1995). A noticeable shift towards the blue is seen in later epochs, suggesting that dust has formed.

has been seen in CCSNe such as 1987A (Emmering & Chevalier, 1989), 2002hh (Welch et al., 2007; Meikle et al., 2006), and 2003gd (Sugerman, 2005), and could be a common occurrence in CCSNe at late times.

1.6 Thesis Goals

In order to address this major question of dust evolution in early galaxies, it is possible to observe nearby CCSNe over the course of many years to search for dust formation and to determine their role as dust producers. Questions still remain as to whether progenitor mass affects dust amounts, if there is a relationship between redshift and dust mass, and the importance of circumstellar interaction in dust processing. It is important to note here that as well as important sources of dust, CCSNe also play a major role as dust sinks due to the destructive properties of the shocks they create. Once we have a clear picture of how current CCSNe play into the dust budget of nearby galaxies, we can have a much better understanding of their role in the early universe, when progenitors may have exceeded 200 $M_{\odot}$. The sample of well studied CCSNe is very small; most observations are taken only within the first few weeks, well before dust formation usually occurs. For those SN with

dust mass estimates, amounts of only 10^{-2}-10^{-5} $M_{\odot}$ have been found (Sugerman et al. 2006, Kotak et al. 2009, for example). This is much smaller than the predicted 1 $M_{\odot}$ per SN needed to account for the amount of dust seen at high-z (Todini & Ferrara 2001, Nozawa et al. 2003).

The goal for my thesis work is to create a broader and more comprehensive sample of well studied CCSNe to determine their role not only for dust production and destruction in the early universe, but in the Milky Way itself. With the use of large ground based and space based telescopes I have amassed a dataset with unprecedented wavelength and temporal coverage centered around quantifying and classifying the dust formation of a few CCSNe. To date only a few Type IIP SNe have been monitored with long-term and extensive spectral and photometric observations, including SN 1990E, SN 1999em, SN 1999gi, SN 2002hh, SN 2003gd, SN 2004et, and SN 2005cs (Maguire et al., 2010, and references therein). I have used the optical photometry to look for signs of deviation from ^{56}Co decay, which powers the SN at late times. The lightcurve can become fainter than this expected luminosity if dust is present and reprocessing the visible light into the IR. Therefore, I have also obtained near simultaneous IR photometry to look for a corresponding brightening in the IR, which will be in the form of an IR excess. Lastly, optical spectroscopy was obtained to search for asymmetries in the emission lines due to dust obscuring the red side more so than the blue side.

I have used these datasets to follow the two CCSNe 2007it and 2007od well over 1000 days to look for signs of dust formation and to better understand the evolution that occurs in these objects. In the following chapters I will discuss in detail the results from my extensive observations. As it is generally thought that stars in the early universe were more massive, this study of nearby SNe will help lay the groundwork for future studies of stars and galaxies at high-z. By thoroughly understanding the dust production and destruction mechanisms in our nearby universe, we will be able to gain a much greater appreciation of dust processes when the universe was very young.

2. Observations and Analysis

2.1 Telescopes and Instruments

For this thesis, I have undertaken an ambitious program to understand how the various dust formation indicators in CCSNe (discussed in Chapter 1) are related, and more importantly how to correctly interpret these indicators to accurately estimate the amount of dust formed in a typical CCSN. Even with very bright SNe, in order to get good temporal coverage both photometrically and spectroscopically, large ground based and space based telescopes are needed, especially at late times when SN luminosities drop dramatically. Telescopes with good wavelength coverage as well as excellent sensitivity and resolution over multiple observations are also required. For these reasons I selected the SMARTS 1.3m telescope for optical photometry at early times when the SNe were quite bright, Gemini/GMOS-S for optical photometry and spectroscopy at early and intermediate times, and Hubble Space Telescope's (HST) ACS/WFC and WFPC2/PC1 for optical photometry at intermediate and late times. For the IR observations I decided to use the IRAC instrument on the Spitzer Space Telescope (SST) and Hubble's WFC3 during the prime dust formation phase in the mid-IR due to the lack of atmospheric interference and their high sensitivity. Molecules, particularly carbon dioxide and water, in the atmosphere of the Earth will absorb many wavelengths of light longer than 1 μm, only allowing transmittance in a few wavelength windows, which makes it very challenging to do IR observations from the ground. This is precisely why space-based IR instrumentation is essential for mid-IR observations. Thankfully, as can be seen in Table 2.1, I was very successful in obtaining observing time on all telescopes, which provided near-simultaneous observations with optical photometry, optical spectra, and infrared photometry that helped to eliminate any ambiguity in the detection of dust formation signatures. In the following sections I will describe the instruments used, as well as the reduction and analysis techniques that were performed on the data.

2.1.1 SMARTS

Early-time optical imaging was obtained in Johnson-Cousins BVI filters with the SMARTS consortium 1.3m telescope at Cerro Tololo Inter-American Observatory (CTIO), Chile. All images were delivered pipeline reduced (discussed below), and were shifted and stacked using the IRAF procedures *imalign* and *imcombine*. Uncertainties were calculated by adding in quadrature the errors associated with the tertiary comparison stars (listed and shown in Appendix A) and the uncertainties in the PSF photometry photon statistics.The SMARTS/ANDICAM 1.3m is a dual-channel, optical-IR imager. The BVRI filters (see Figure 2.2) on the CCD have a field of view (FOV) of ∼6x6 arcminutes and a pixel scale of 0.369-arcsec/pixel (DePoy et al., 2003, see Figure 2.1). The aperture of this instrument, with a limiting magnitude of ∼21 in the V band (with very long exposures times), and seeing $\geq$ 0.5", make the 1.3m only practical for early times (less than $\sim$ 150 days).

Table 2.1: Summary of Approved Proposals, PI Andrews

Telescope	Instrument	Proposal ID	Objects	Hours
SST	IRAC-warm	70201	SN 2010jl	0.8
SST	IRAC-warm	70008	SNe 2007it, 2007od	9.5
Gemini-S	GMOS	2010A-DD-3	SN 2007it	1.9
SST	IRAC-warm	60071	SNe 2007it, 2007od, 2007oc	6.3
Gemini-S	GMOS	2009B-Q-1	SNe 2007it, 2007od, 2007oc	10.2
Gemini-S	GMOS	2009A-Q-49	SNe 2007it, 2007od, 2007oc	24.5
HST	WFC-2, ACS, WFC3	11603	SNe 2007it, 2007od, 2007oc	21
SST	PUI, MIPS	500353	SN 2007od	0.5
Gemini-S	GMOS	2008B-Q-45	SNe 2007it, 2007od, 2007oc	9.3
SST	IRAC	50534	SNe 2007it, 2007od, 2007oc	4.3
Gemini-S	GMOS	2008A-DD-2	SNe 2007od, 2007oc	2.5
Gemini-S	GMOS	2008A-Q-24	SN 2007it	11

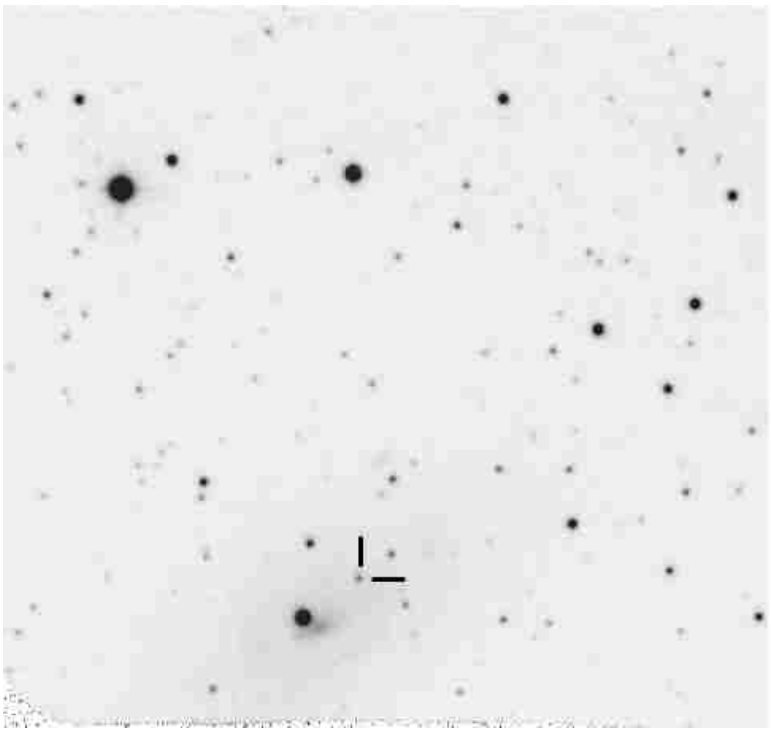

Figure 2.1: Schematic of a SMARTS field of view of NGC 5530, SN 2007it is marked.

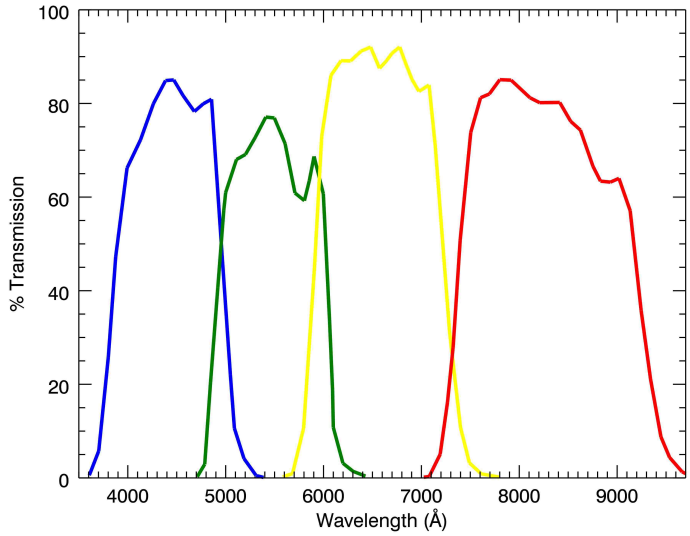

Figure 2.2: Transmission curves for the BVR_cI_c Johnson-Cousins Filters used by the SMARTS 1.3m telescope.

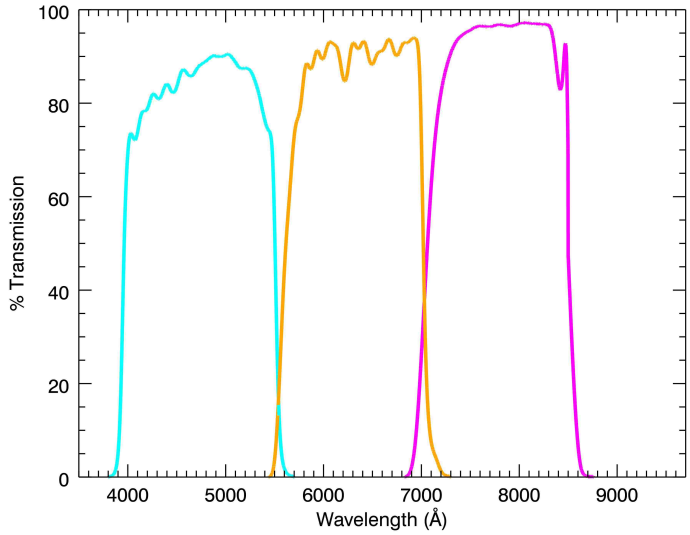

Figure 2.3: Transmission curves for the g′r′i′ filters used by Gemini-S.

2.1.2 Gemini South

The Gemini Multi-Object Spectrograph (GMOS) offers both long slit and multi slit spectroscopy, as well as optical imaging on the 8.0m mirror. The FOV is 5.5 arcmin^2 over 3 CCD chips, with two 2.8 arcsec (39 pixel) gaps between the detector chips, and a scale of .0727 arcsec/pixel (Hook et al., 2004, Figure 2.4). For optical imaging, GMOS uses u′g′r′i′z′ Sloan Filters (see Figure 2.3), with a limiting magnitude of around 26 for the g′ filter. The g′r′i′ images were reduced and stacked using the IRAF *gemini* package. The instrumental g′r′i′ magnitudes were transformed to standard Johnson-Cousins VRI using the following transformations:

V = 0.7111 × g′ - 0.0829 × r′ + 0.3728 × i′ + *zero point*
R = 0.7540 × r′ + 0.2664 × i′ + *zero point*
I = -0.2786 × r′ + 1.2531 × i′ + *zero point*

(Welch et al., 2007; Fukugita et al., 1996). For each night the errors were calculated by adding in quadrature the transformation uncertainty quoted in Welch et al. (2007), uncertainty from photon statistics, and the zero point deviation of the standard stars for each epoch. There are some small discrepancies between the SMARTS and Gemini I magnitudes, especially in SN 2007it, that are likely due to the bandpass of the Cousins I filter covering part of the Ca II IR-triplet around 8500Å that is not covered by the Gemini i′ filter. This is shown in Figures 2.2 and 2.3, and would cause the SMARTS photometry to appear brighter due to the added Ca II flux.

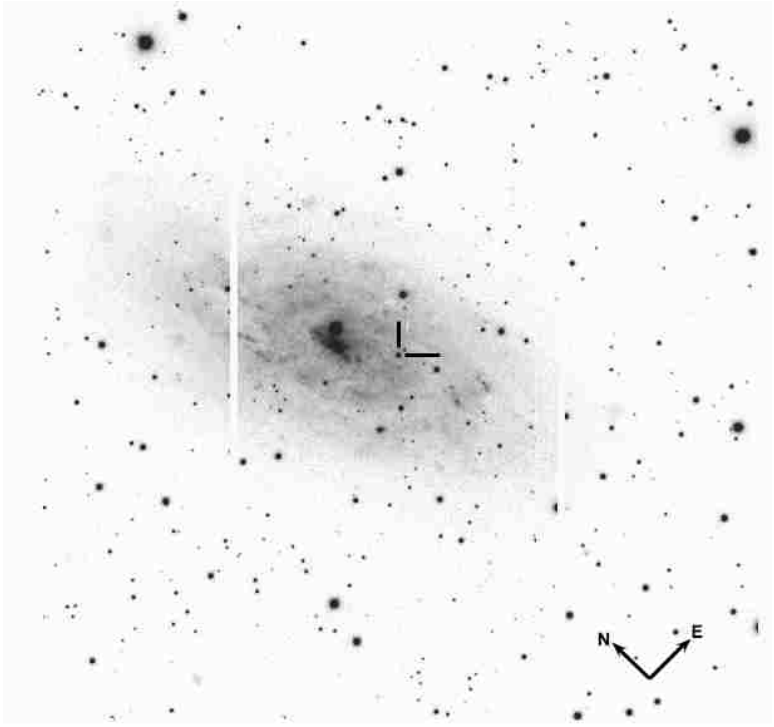

Figure 2.4: Schematic of a Gemini/GMOS field of view of NGC 5530. SN 2007it is indicated.

For long-slit spectroscopy, GMOS uses changeable masks with slits of different widths

with an average limiting magnitude of about 22.5 magnitudes. This is ideal for observing SNe well past 500 days. For the Gemini/GMOS South epochs, three integrations of 900 or 1800 seconds (depending on the faintness of the object) were obtained in longslit mode using grating B600 and a slit width of 0.″75. Central wavelengths of 5950, 5970, and 5990 Å were also chosen to prevent important spectral features from falling on chip gaps. A 2x2 binning in the low gain setting was used. Spectra were reduced using the IRAF *gemini* package. Figure 2.5 shows a 2D unextracted spectrum of NGC 5530. The sky subtraction regions were determined by visual inspection, and included 30 pixels on either side of the SN. The spectra were extracted using 20 rows centered on the SN. The spectra from each individual night were averaged and were corrected for the radial velocity of the host galaxy.

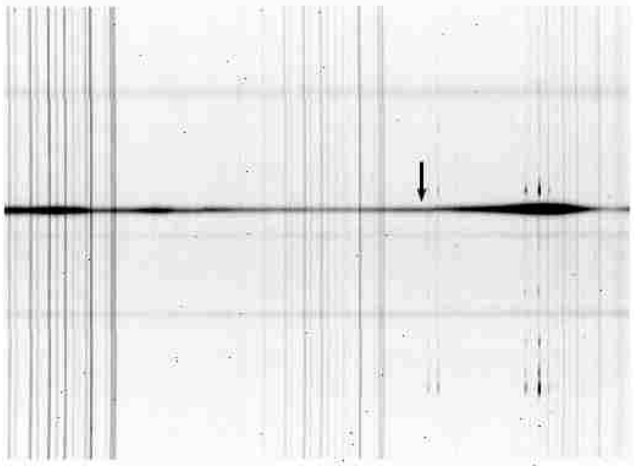

Figure 2.5: Raw GMOS 2D spectra prior to extraction of NGC 5530. Since the x-axis is wavelength, SN 2007it runs from left to right and is indicated by an arrow. The broad region near the right-hand side is the Hα emission.

2.1.3 Hubble Space Telescope

Extragalactic CCSNe are faint (V>21) 1-2 years after outburst, and since they are located within the disks of their host galaxies, the fields are often crowded and have high and variable background surface brightness. Thus the high resolution and sensitivity of HST and the ACS/WFC (Advanced Camera for Surveys/Wide Field Camera) make it the perfect instrument (Shaw et al., 2009). Due to problems with ACS and the setback of the HST servicing mission to late May 2009, during Cycle 17 I also made use WFPC2/PC1 in lieu of ACS/WFC for my first observations of SNe 2007it and 2007oc. ACS/HRC is perfect for crowded fields (see Figure 2.6) because the image scale of 0.025″/pixel and the lack of seeing constraints makes it possible to be able to distinguish individual stars. Although WFPC2/PC1 has a lower resolution at 0.046″ per pixel, if extra exposure times are taken, and a 4-point dither is used, it can be as effective as using ACS/WFC for signal-to-noise (S/N). Both instruments have approximate BVI filters (F450W, F606W, and F814W), allowing comparison with both SMARTS and Gemini optical photometry. The FOV's for both WFPC2 and ACS are shown below in Figure 2.6.

One epoch of SN 2007it photometry was obtained with the WFPC2/PC1 camera on HST in the F450W, F606W, and F814W filters. These images were delivered pipeline reduced,

but undrizzled. Stacking and cosmic ray removal was accomplished using the Pyraf task *multidrizzle*. Transformation into the standard Johnson-Cousins BVI was done using methods outlined by Holtzman et al. (1995). Late time images were obtained with the Wide Field Camera (WFC) on HST/ACS using the F435W, F606W, and F814W filters. These images were pipeline reduced, including drizzling and cosmic ray removal. Transformations to the Johnson-Cousins BVI system were accomplished using Sirianni et al. (2005). The large bandpass of the F606W filter includes the 6563 Å Hα emission, which is the main source of the late-time luminosity. We believe this causes the transformed Johnson V magnitude from HST to appear brighter than the V magnitude obtained from the Gemini images. In the Gemini filter set, r$'$ contains the Hα flux, and is a very small component to the Johnson V transformation but a large component to the R transformation. Therefore the R magnitude from Gemini would contain the Hα emission whereas Hα would be present in the V magnitude from HST. This is discussed in more detail in Chapters 3 and 4.

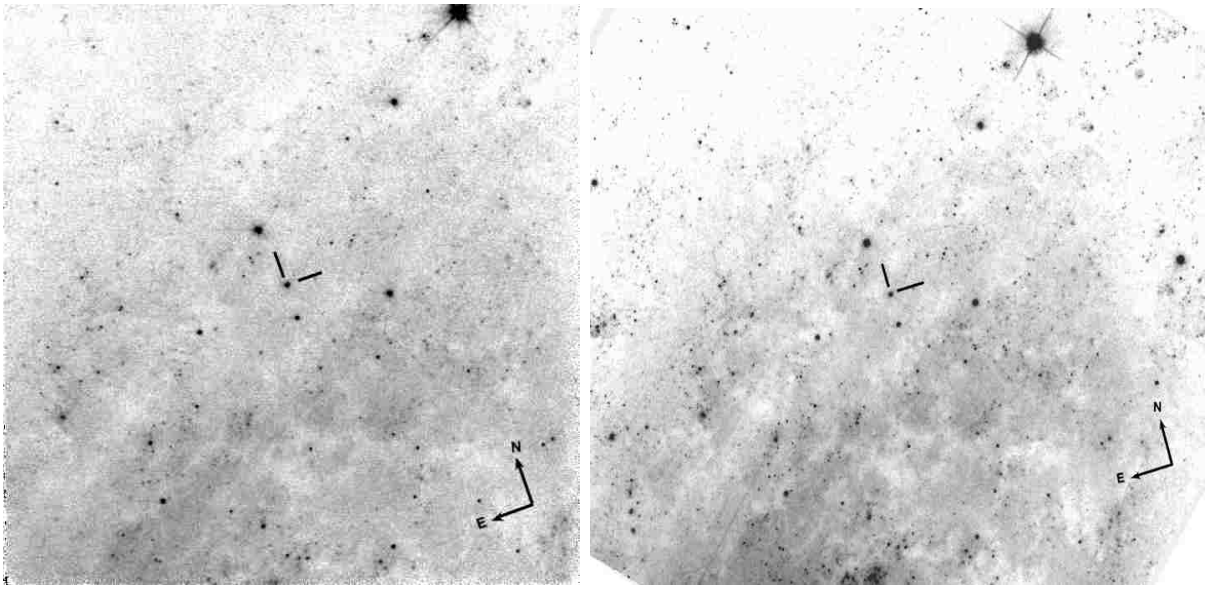

Figure 2.6: FOV of HST WFPC2 (left) and ACS (right) of NGC 5530. The scales have been matched to WFPC2, and SN 2007it has been marked in each.

2.1.4 Spitzer

Because of the brightening in the infrared that occurs during the onset of dust formation, an instrument is needed that can easily detect mid-IR emission from dust grains at distances of ∼20 Mpc. The earth's atmosphere is not conducive to detecting mid-IR from objects in space (especially in the wavelength range between 4-8 μm), so a space based telescope is the most effective way of detecting these infrared excesses. Spitzer's IRAC (Infrared Array Camera) is composed of four channels that provide simultaneous 5.2$'$ x 5.2$'$ images at 3.6, 4.5, 5.8, and 8.0 μm (Fazio et al., 2004). Figure 2.7 shows the FOV of UGC 5530 in the 3.6 μm band. These wavelengths are all in the mid-infrared regime, which is the wavelength band in which warm dust shines most brightly, making it ideal for this project. Unfortunately Spitzer went into warm mission mode in April 2009 from loss of coolant, which cut the detection range to 3.6 and 4.5 μm for all late-time observations.

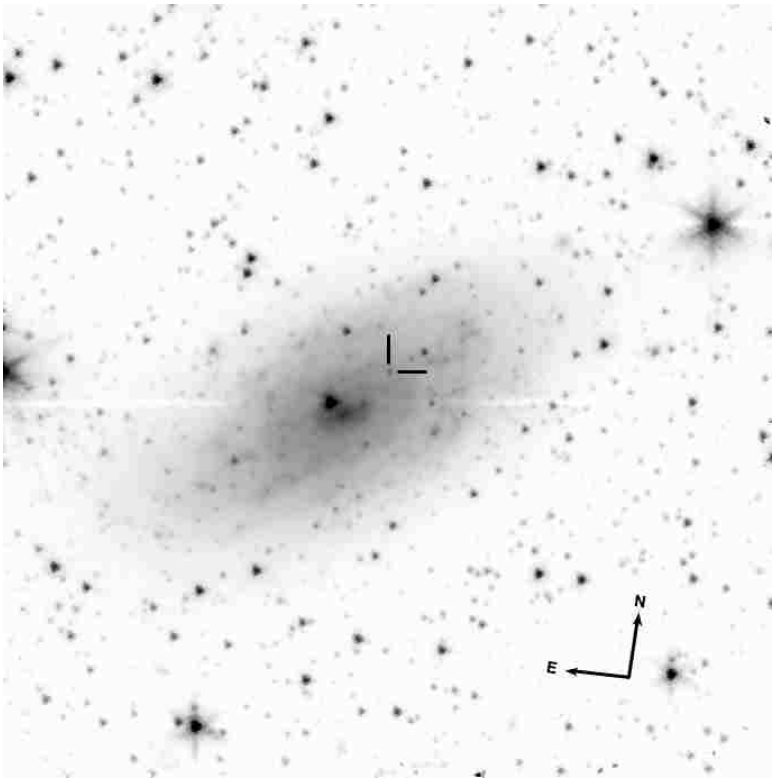

Figure 2.7: 3.6 μm image of NGC 5530 from Spitzer Space Telescope. SN 2007it is indicated in the center.

The Spitzer IRAC images were mosaiced and resampled using standard MOPEX procedures to improve photometric quality (Makovoz & Marleau, 2005). The photometry was done for the mid-IR the same way as for other wavelengths, using *psf* and *allstar* (described below) to determine fluxes from the SN. Standard instrumental PSFs (called PRFs for Spitzer) for the specific location of the SN on the chip, used for psf photometry, were provided through the Spitzer Data Center. The flux unit of the IRAC mosaiced images is in MJy/sr instead of counts/second as in the optical images. This value can then be converted to μJy/pixel using the quoted conversion factor of 1 MJy/sr = 33.84μJy/pixel for a 0.6″x 0.6″image in IRAC.

2.2 Data Reduction

Basic reduction of most raw CCD images include a bias subtraction, a dark subtraction, flat fielding correction, and a cosmic ray correction. Thankfully, numerous telescopes now offer a pipeline which will correct all raw images for these issues and present reduced images for collection. If multiple frames of the object are taken during one observation, oftentimes these images need to be aligned and stacked in order to produce one summed image with high S/N. All of these tasks can be done in the software system IRAF (Image Reduction and Analysis Facility.) These tasks remove any artifacts that may be associated with the telescope, the CCD, or the filters, and leave us with data quality images. Photometry is then done on these images and values are output in either instrumental magnitudes or fluxes that are unique to every instrument/filter combination. In order to convert these instrumental magnitudes to the standard system, we will then need a set of equations and/or standard stars. A $BVRI$ photometric sequence of tertiary standard stars was derived for each SN, and a table of magnitudes for these standards as well as finder charts for each is located in Appendix A.

Photometry itself can be done in one of two ways, either by aperture photometry or point spread function (PSF) photometry. Aperture photometry works well with non-crowded fields, especially those in which there are published standard star magnitudes. The method is simple; an aperture radius in pixels is chosen which incorporates the star, with very little surrounding sky, and the counts are simply added up. At the same time an annular region outside of the aperture radius is chosen to measure the sky background counts, which is then subtracted from the counts in the object aperture, giving a true value for counts. IRAF has a reduction task called *phot* in the *DAOphot* package which does this automatically when the position of the star, along with the values desired for aperture and sky annulus, are given.

Oftentimes the object is in a crowded field where it is possible that an aperture may include another star. For these situations it is best to use another photometry method called PSF fitting. With this method an average PSF is created using bright, isolated stars in the field. These stars are presumed to have a reliable and singular PSF, with no interference from neighboring stars. This average PSF is then fit to the other stars which may not be isolated and may not have an accurate PSF. This allows us to be able to distinguish one star from another, and to measure the magnitudes. In IRAF, PSF photometry is slightly more complicated than aperture photometry. To begin with *phot* must be run on the PSF stars in order to get an estimate of the background counts. Then the selected stars must be input into the iraf task *psf* which allows interactive selection of clean and accurate PSF's, and then fits an analytic function to create one master PSF profile. This profile can then be fit to any star in the field using a task called *allstar*, which outputs a file with an instrumental magnitude. Space telescopes like HST and SST will even provide standard PSFs for particular filter and chip position combinations which eliminates the need for creating a PSF profile from nearby

stars. Although PSF fitting seems slightly more involved, it does tend to yield better results, even in non-crowded fields, therefore I have chosen to use it for the photometry of all of my observations.

The spectra taken with Gemini/GMOS are distributed as raw, two dimensional images (Figure 2.5). Gemini has also developed an IRAF package specifically for the reduction of GMOS spectral data. All spectra are taken with GCal flats and CuAr spectra, which are used to calibrate the transformation from pixel to wavelength. Bias frames are also taken and distributed with the data. The normal reduction and extraction procedure follows the form *gbias, gsflat, gsreduce, gswavelength, gstransform, gsskysub* and *gsextract.* The first task removes the bias from all the images, while *gsflat* creates a flat field for the GMOS spectra based on the GCal flat lamp exposure. The next task, *gsreduce* does numerous reduction techniques, including overscan correction, mosaicing, and approximate wavelength calibration. *Gswavelength* then takes the CuAR files and creates an exact wavelength calibration for the spectra, which is then used in *gstransform* to calibrate the spectra. Finally the sky (in the 2D spectra, the area above and below the spectrum) is subtracted using the task *gsskysub*, and a final extracted, 1D spectra is created with *gsextract*. For the final analysis, the spectra from each night are averaged and then normalized for comparison with spectra from other nights, allowing easy determination of any shifts or asymmetries in the lines (Welch et al. 2007).

2.3 MOCCASIN Monte Carlo Radiative Transfer Code

In order to better understand the amount and composition of the dust forming within the SNe I used our 3D Monte Carlo radiative transfer (RT) code MOCASSIN (Ercolano et al., 2005, and references therein). MOCASSIN is a three-dimensional Monte Carlo radiative-transfer code that is capable of modeling non-spherical geometries, clumpy density distributions, and non-central energy sources. It allows for the existence of gas and dust that may already be present in most physical systems, and uses Mie scattering to determine absorption and scattering efficiencies. It is capable of handling multiple grain species and distributions, as opposed to the more commonly used approximation of a group of grains as one grain. I have chosen to model three different geometries in which the dust is distributed either uniformly within a spherical shell surrounding the SN, with the addition of clumps scattered throughout the shell, or in a torus at some inclination around the SN. These will be known as "smooth", "clumpy", and "torus" models, respectively.

The "smooth" model has the dust uniformly distributed throughout the shell according to a r^{-2} density profile, while the "clumpy" model reflects an inhomogeneous distribution of spherical clumps embedded within an interclump medium of density ρ. The irradiating photons are only produced in the interclump medium, while the clumps are assumed to be dark (see Ercolano et al. (2007) for further discussion of this issue). For the torus models, densities are specified for the inner and outer walls, with the dust distribution falling off linearly between the two radii. Relying on previous modeling done by Sugerman et al. (2006), Meikle et al. (2007), and Kotak et al. (2009) I have used a standard MRN (Mathis Rumpl Nordsieck) grain size distribution of $a^{-3.5}$ between 0.005 and 0.05 μm (Mathis et al., 1977) for all three scenarios.

The ejecta provides the photons for heating the dust. It is modeled as a diffuse energy source spread throughout a shell with size R_{in} and R_{out}. The dust is mixed in with the ejecta either homogeneously or in a clumpy distribution. The main input parameters for the model are the ejecta temperature and luminosity, the inner and outer radii of the shell, and the mass of dust present. Initial values of the luminosity, temperature, and approximate

size of the dust shell are based on the results of blackbody analysis. Using the distance and luminosity of the SN in different wavelengths at a specific epoch a blackbody temperature and radius can be fit both to the visible and IR components using Planck's function. Tuning the dust mass, along with slight variations in the other parameters, allowed me to obtain a good fit to the optical and Spitzer/IRAC points. The percentage of amorphous carbon and silicates is determined through many trials to find the best fit, but the parameters used to fit the dust emission of other CCSNe were used as starting points for the fits here. An elevated brightness of the 8.0 μm filter is usually an indicator of the presence of a strong silicate feature and therefore a higher percentage of silicate dust. A more in-depth discussion in relation to each SN is discussed in Chapters 3 and 4.

3. SN 2007od [1]

3.1 Introduction

SN 2007od is located in UGC 12846 at a distance of 24.5 Mpc (Immler & Brown, 2007). It was discovered on 2007 November 2 with $R \sim$14.4 mag (Mikuz & Maticic, 2007), and two days later was confirmed spectroscopically as a normal Type II SN most closely resembling SN 1999em at 10 days past explosion (Blondin & Calkins, 2007). Based on this, we assume an explosion date of 2007 October 25 (JD 2454398) throughout this chapter. The new observations reported in this chapter are summarized in Table 3.1. We have obtained visible spectroscopy and photometry spanning days 57-811 as well as mid-infrared photometry on days 300, 455 and 667 of SN 2007od.

Table 3.1: Observation Summary of SN 2007od

Day	JD	Telescope	Instrument	Exposures	Time/Exposure *(s)*
57	2454455	SMARTS 1.3m	ANDICAM	5	20
232	2454630	Gemini South	GMOS Spectra	3	900
232	2454630	Gemini South	GMOS Imaging	3	20
300	2454698	Spitzer	IRAC	12	100
309	2454707	Gemini South	GMOS Spectra	3	900
309	2454707	Gemini South	GMOS Imaging	1	60
348	2454746	Gemini South	GMOS Spectra	3	900
348	2454746	Gemini South	GMOS Imaging	2	60
455	2454853	Spitzer	IRS PUI	9	15
458	2454856	Gemini North	GMOS Spectra	3	900
458	2454856	Gemini North	GMOS Imaging	1	60
461	2454859	Spitzer	IRAC	12	100
471	2454869	Spitzer	MIPS	16	30
659	2455057	HST	ACS/WFC	4	98
667	2454865	Spitzer	IRAC	12	100
672	2455070	Gemini South	GMOS Spectra	6	1800
672	2455070	Gemini South	GMOS Imaging	2	60
699	2455097	Gemini South	GMOS Spectra	6	1800
709	2455107	HST	ACS/WFC	4	98
811	2455109	HST	ACS/WFC	4	98

[1] Andrews et al. (2010)

3.2 Lightcurve Evolution

A typical Type IIP SN lightcurve shows a plateau for the first ∼60-100 days, followed by a sharp drop in luminosity of ∼1.5-3 mag as the SN transitions into the nebular phase, after which the lightcurve exhibits an exponential decline powered by ^{56}Co decay (Woosley & Weaver, 1986). The lightcurve of SN 2007od (Figure 3.1) shows a normal plateau phase followed by an exceptionally large drop in brightness as it is entering the nebular phase. The last photometry before the gap was obtained on day 82 (Chornock 2009, personal communication). If we assume the end of the plateau phase took place shortly after that time and we extrapolate the slope of the ^{56}Co decay backwards into the gap (days 82-232) when no photometry is available, we find that the V brightness fades a minimum of 4.5 mag over the typical twenty day drop period (Elmhamdi et al., 2003a). Woosley & Weaver (1986), and more recently Kasen & Woosley (2009), have suggested that if only a small amount of ^{56}Ni is synthesized in the SN explosion the lightcurve will show a steep drop between the plateau and nebular phases due to a lack of sufficient thermal energy. Generally, such a steep drop is only seen in low-luminosity (M_v ∼-14) SNe such as 1999br, 1999eu and 2005cs, that have very low inferred ^{56}Ni masses (2 – 8 x $10^{-3}M_{\odot}$) (Pastorello et al., 2004). SN 1994W, which dropped ∼3.5 mag from days 110 to 122 (Sollerman et al., 1998) is the only other luminous (M_v ∼-18) Type IIP besides SN 2007od to show such a steep drop in brightness. Its ^{56}Ni mass was estimated to be ∼2.6 × $10^{-3}M_{\odot}$. Sollerman et al. (1998) suggested that after its 3.5 mag drop from the plateau, SN 1994W declined much faster than the ^{56}Co decay once in the nebular phase, possibly due to dust formation.

Table 3.2: Optical Photometry of SN 2007od

Day	V	R	I
57	14.86 ± 0.04	-	14.17 ± 0.03
232	21.32 ± 0.04	20.43 ± 0.02	20.21 ± 0.03
309	22.05 ± 0.05	21.36 ± 0.03	21.10 ± 0.05
348	22.44 ± 0.05	21.80 ± 0.03	21.54 ± 0.05
458	23.51 ± 0.12	22.66 ± 0.07	22.77 ± 0.15
659	23.64 ± 0.18	-	24.08 ± 0.35
672	24.67 ± 0.15	23.82 ± 0.10	24.10 ± 0.25
709	23.68 ± 0.21	-	24.22 ± 0.50
811	23.76 ± 0.20	-	24.24 ± 0.44

After day 458 the lightcurve of SN 2007od shows a deviation from ^{56}Co decay in the form of a flattening of the lightcurve between days 659 and 811. By day 811, assuming a constant brightness has been maintained from day 672, the difference in an extrapolated ^{56}Co decay is ∼2.2 magnitudes in V. At late times, the Gemini and HST V magnitudes differ significantly due to differences in the filter bandpasses as discussed in Section 2. However, the constancy of the three epochs of HST/ACS V and I photometry from day 659 to 811 show that the flattening of the lightcurve is real. It is likely being caused by a light pulse from the SN reflecting off of surrounding dust and creating a light echo. Given the distance of the SN (24.5 Mpc), the platescale of the WFC detector ($0.''05$ pix^{-1}) and the FWHM of the stellar PSF (1.9 pix), a source could have a spatial extent on the plane of the sky of up to $0.12''$or 46 lt-yr and still be unresolved on the detector. In particular, we find through

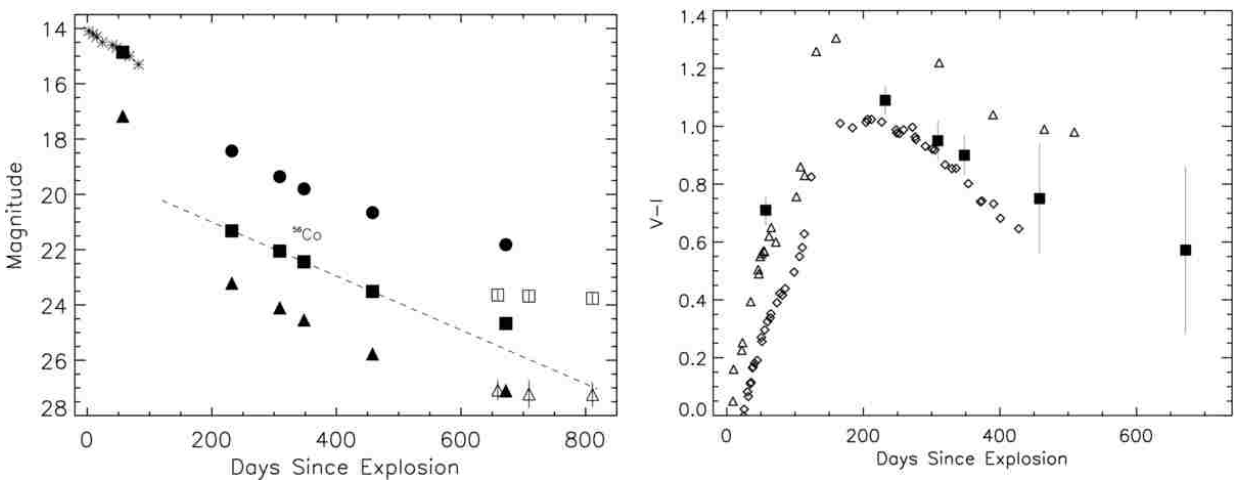

Figure 3.1: **Left:** Johnson-Cousins VRI lightcurves of SN 2007od. R points are shown as circles and have been shifted up 2 mag, V are shown as squares, and I as triangles shifted down 3 mag. The filled symbols are from Gemini/GMOS and the open symbols from HST ACS/WFC. Additional photometry of SN 2007od obtained with no filter is plotted (asterisks). The uncertainties are listed in Table 3.2, and are in most cases smaller than the symbol size. The dashed line represents the ^{56}Co decay. Note the drop of ∼4.5 mag in V in 20 days, which is large for a Type IIP SN. The disagreement in V between Gemini and HST at late epochs is most likely due to filter bandpass differences (see text). **Right:** Evolution of the Gemini $V - I$ color of SNe 2007od (filled squares), 1999em (triangles), and 2004et (diamonds) (Elmhamdi et al., 2003b; Sahu et al., 2006). The $V - I$ colors of SNe 1999em and 2004et have been corrected for foreground extinction.

experimentation that a source with the flux of this SN and with a FWHM up to 1.2 times that of the PSF will not leave detectable residuals when subtracted away, therefore we allow the physical size of the emitting region to be up to 0.12″. Using the light echo equation (Couderc, 1939; Sugerman, 2003), dust could be up to 475 lt-yr in front of the SN on day 811 and still remain unresolved in the HST imaging. Thus, the echoes could be produced from either circumstellar or interstellar dust. Given that the foreground extinction to the SN is low ($A_V \sim 0.4$), any dust producing a light echo should be optically thin. Typically, the contribution from a light echo becomes significant when a SN has faded ∼8 mag from maximum (Patat et al., 2006). SN 2007od was more than 10 mag below maximum light by day 672 when the contribution of the echo to the lightcurve became significant. A qualitative comparison of the lightcurve and evolution at late times of SN 2007od to models by Patat (2005) suggest that the echo is more likely due to an interstellar sheet than circumstellar dust. We discuss possible contributions of an echo to the spectral evolution of SN 2007od in Section 3.2.

As seen in Figure 3.1, the evolution of the $V - I$ colors is normal for a dust forming Type IIP SN. We have only included the $V - I$ colors from the Gemini observations due to the bandpass considerations of HST described in Section 2.1.3. At the time of dust formation, previous photometry of SNe 1999em and 2004et showed only small (<0.1 mag) changes in their $V - I$ colors. The $V - I$ color evolution of SN 2007od before and after the gap in observations (days 82-232) when we think dust formation began, is consistent with these

other SNe. The lack of change in the $V - I$ color evolution indicates that, in general, the color evolution is not sensitive to dust formation. This is likely caused by either a very small amount of dust being formed, or larger amounts forming in clumps. If the dust is clumpy, then the color evolution would not reflect the optical depth of dust present and the colors would not be as reddened as they would be if the dust were uniformly distributed e.g., (Witt & Gordon, 1996).

3.3 Spectral Evolution

The spectral evolution of SN 2007od shows behavior not previously seen in other SNe. Figure 3.2 shows the full optical spectrum of SN 2007od at 10, 232, and 458 days. Early-time spectra showed SN 2007od to be a normal Type II SN with a blue continuum, broad Hα emission with a P-Cygni profile, and an expansion velocity of $\sim$10000 km s^{-1} (Blondin & Calkins, 2007, Chornock 2009, personal communication). Other notable spectral features at early times include broad Hβ emission, weak Na I D $\lambda\lambda$5890,5896 absorption, and [O I] $\lambda\lambda$6300,6363 emission that was weaker than that normally seen in Type II SNe. There was no sign of either a narrow (FWHM $\sim$ 200 km s^{-1}) Hα component nor X-ray emission (Blondin & Calkins, 2007; Immler & Brown, 2007), typically seen in a Type IIn SN. If present, the X-ray luminosity of SN 2007od was $< 1.0 \times 10^{40}$ erg s^{-1}, significantly smaller than luminosities measured in Type IIn SNe such as 2006jd and 2007pk (Immler et al., 2007a,b).

By the time of the first Gemini/GMOS epoch (day 232) the spectrum of SN 2007od showed evidence for strong interaction with its CSM, an event usually associated with Type IIn SNe. The Hα emission profile had changed dramatically from the early-time spectra, with the single broad component evolving into at least three intermediate width (FWHM $\sim$ 1700 km s^{-1}) emission components on top of a fainter, broader emission component (Figure 3.3). Two of these intermediate width components are arranged symmetrically about zero velocity at $\pm$1500 km s^{-1} and the third, which becomes more prominent at later epochs, lies at -5000 km s^{-1}. We should note that the narrow emission at zero velocity is HII emission from the host galaxy not associated with the SN. Underlying the three intermediate width components, the broad Hα emission present in the early-time spectra can still be seen, and it is likely that it is responsible for the broad red wing of the Hα emission profile (see Figure 3.3). Broad, blended Fe II emission between 5100-5400 Å similar to that seen in SN 1998S (Pozzo et al., 2004) appeared by day 232, and [Ca II] $\lambda\lambda$7291,7324 emission became prominent by day 458 (Figure 3.2).

A similar multi-component structure was seen in the Hα profile of SN 1998S. Unlike SN 2007od, SN 1998S was classified as a Type IIn, and showed both broad and narrow Hα emission components at early-times due to the expanding ejecta and photoionized CSM material, respectively. The narrow component disappeared before day 108 (Leonard et al., 2000), and sometime before day 250, a triple-peaked Hα emission profile had developed (Gerardy et al., 2000) (Figure 3.3). The three intermediate width components persisted in SN 1998S from approximately day 250 to day 660, exhibiting a progressive fading of the red and central components with respect to the blue component; a phenomenon that was attributed to dust formation (Gerardy et al., 2000). The timescale for the evolution of the SN 1998S spectrum is similar to that of SN 2007od, which showed a single broad Hα emission component from days 10-114, followed by a period (114-232 days) when the SN was unobservable, and finally the emergence of multiple-component emission by day 232. In SN 2007od, the blueshifted component at -1500 km s^{-1} is much stronger than its corresponding component at +1500 km s^{-1}. Like SN 1998S, the simplest explanation for this asymmetry

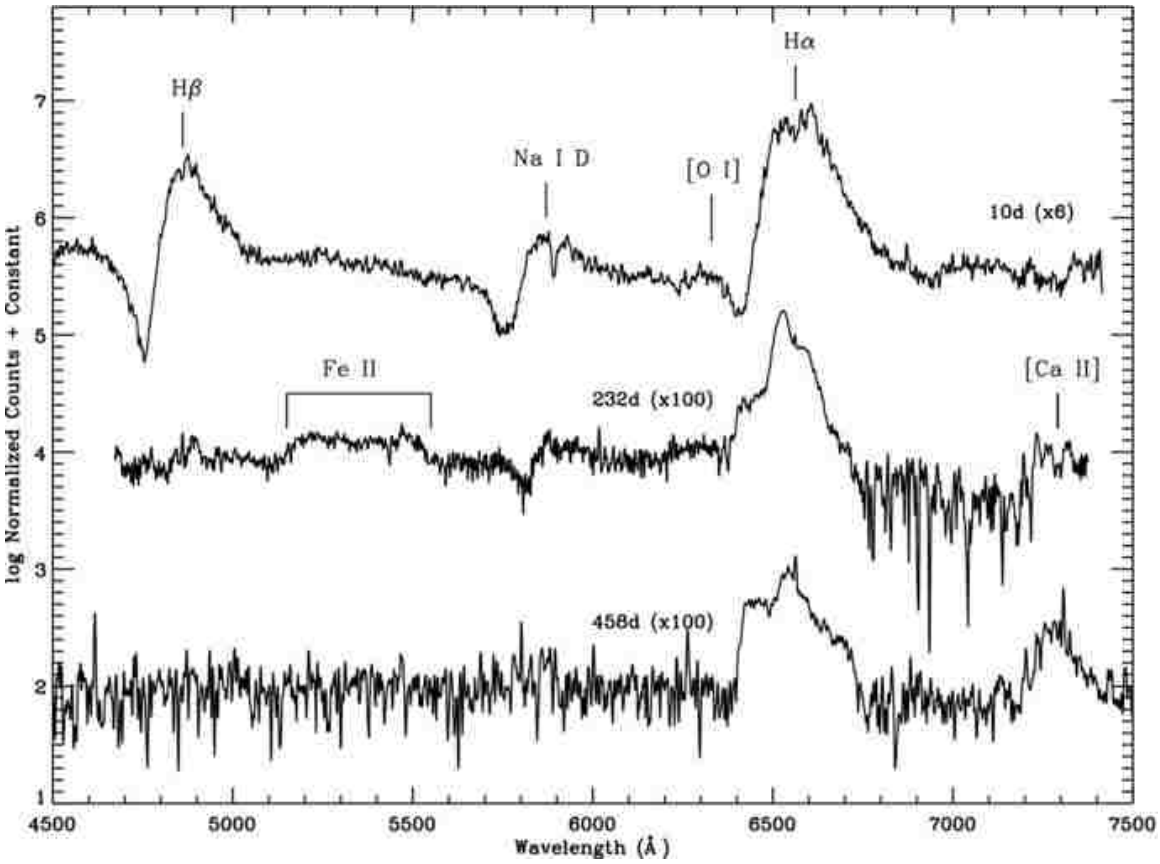

Figure 3.2: Optical spectra of SN 2007od on days 10, 232 and 458. All spectra have been normalized to the continuum and are shifted vertically by a constant. See text.

is that newly formed dust is extinguishing the redshifted, far-side emission more than the blueshifted, near-side emission. The ratios of the inner peak heights would require an optical depth of approximately 1.0 at Hα for the asymmetry to be attributable to dust attenuation. If the dust existed in the CSM before the SN explosion, then it would lie outside of the ejecta and all of the emission components would be equally reddened. It is thought that the outer peaks in the Hα profile of SN 1998S originated in the interaction of the ejecta with a circumstellar ring or torus (Gerardy et al., 2000; Leonard et al., 2000; Pooley et al., 2002; Pozzo et al., 2004; Fransson et al., 2005). If we assume the same is true of the asymmetric inner peaks of SN 2007od, then there must be dust between the source of the near-side (blueshifted) and the far-side (redshifted) emission components in the torus (Figure 3.4). Moreover, if this dust is forming in the CDS, as was suggested by Pozzo et al. (2004) for SN 1998S, then the emission would likely be coming from a radiative forward shock (Pozzo et al., 2004; Fransson et al., 2005) as one would expect equal attenuation of both redshifted and blueshifted emission originating in the reverse shock. It is also worthwhile to note that Kotak et al. (2009) has recently alluded to CSM interaction producing a similar multi-component Hα profile in SN 2004et, but occuring at least 400 days after it was seen in SNe 1998S and 2007od.

In SN 2007od, the $\pm$1500 km s^{-1} peaks appear sometime between day 114 and 232. Given the maximum velocity of the ejecta of 10000 km s^{-1}, this constrains the distance of

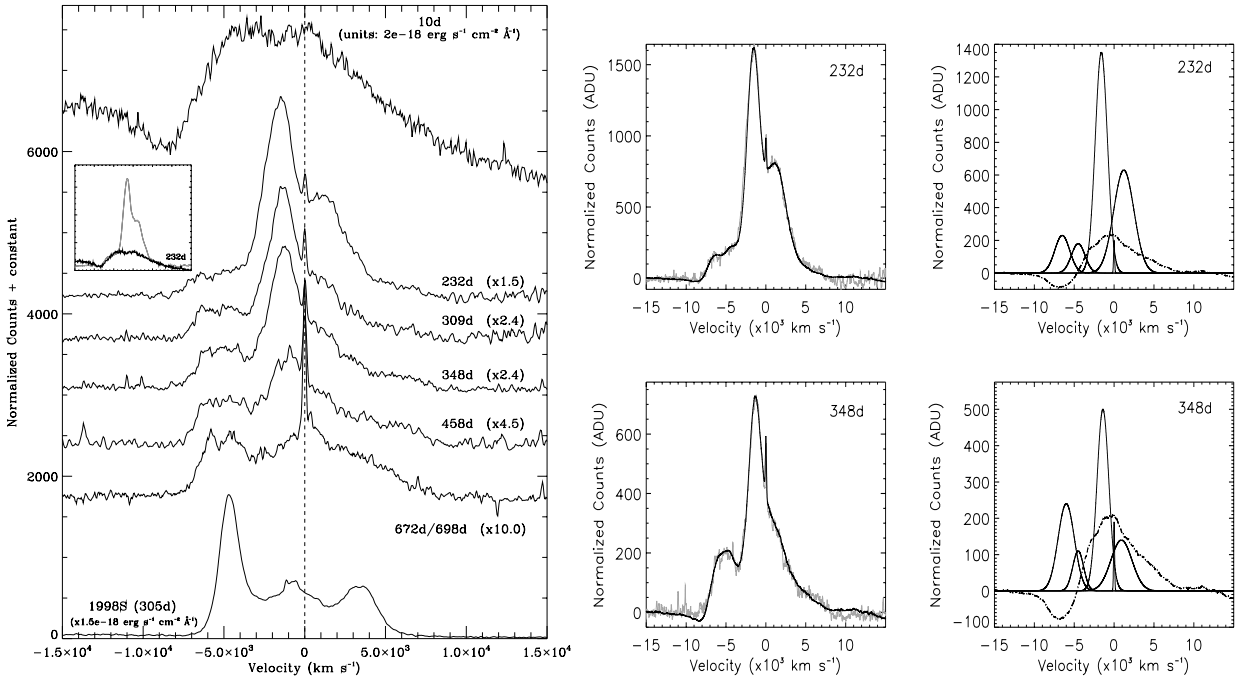

Figure 3.3: **Left:** Spectral evolution of the Hα profile of SN 2007od. The -5000 km s^{-1} component is easily visible by day 309, and the inner $\pm$1500 km $^{-1}$ components disappear by day 672/699. For comparison, the Hα profile of SN 1998S (day 305) has been included (Pozzo et al., 2004). **Right:** Deconvolution of the Hα profiles on day 232 and 309 are shown on the right side panels, and the fit is shown as a black line over the spectrum on the left side panels. The dashed-dotted line indicates the day 50 profile, which is the residual broad emission still seen at later times. Neither the $\pm$ 1500 or -5000 km s^{-1} components can be produced by the early time spectra, indicating they are the result of CSM interaction. The double gaussian fit to the -5000 km s^{-1} component is likely caused by density enhancements in the CSM. The day 672/699 spectra, shown on the left, is largely powered by light echo emission, which contributes only a tiny amount to the early-time spectra.

the inner radius of the CSM responsible for these profile peaks to $\sim$700-1300 AU. Assuming a progenitor wind of 10 km s^{-1}, this CSM was formed during a mass loss event ending 300-600 years prior to the SN explosion. With the emergence of the -5000 km s^{-1} components between days 114 and 309, a similar analysis places this CSM at 700-1700 AU and the formation period between 300-800 years prior to explosion.

The appearance of the asymmetric components between days 114 and 232 implies that dust formation began much earlier than typically seen for non-interacting CCSNe. These SNe (SN 1987A, 2003gd, 2004et) showed developing asymmetries between days 300 and 600 post explosion due to dust condensation in the ejecta (Lucy et al., 1989; Sugerman et al., 2006; Sahu et al., 2006). Furthermore, the [Ca II] λ7291 emission profile in the day 458 spectrum shows only the one broad component, with no intermediate-width components present (Figure 3.2). This implies that the complex emission seen in Hα is arising in the hydrogen-rich CSM lost from the star before the explosion and not in the metal-enriched

ejecta (Gerardy et al., 2000). These observations are more consistent with dust formation in the CDS as has been suggested in SN 1998S (Pozzo et al., 2004; Fransson et al., 2005).

The Hα profile of SN 1998S also showed a third peak near zero velocity that has been attributed to the interaction of the ejecta with a spherical distribution of shocked CSM clouds (Gerardy et al., 2000; Leonard et al., 2000; Pooley et al., 2002; Pozzo et al., 2004; Fransson et al., 2005). In the case of SN 2007od, Figure 3.3 also shows the emergence of a third peak at -5000 km s^{-1} that was hidden by the broad ejecta emission on day 232. This blue peak becomes increasingly more prominent as the broad underlying ejecta emission begins to fade over time. By day 699, when we believe the light echo is contributing significantly to the flux, this feature is still prominent. Because a light echo depicts only the early-time emission, it is not possible to explain the -5000 km s^{-1} peak with a light echo scenario. The nature of this third peak represents the starkest difference between SNe 2007od and 1998S. As previously mentioned, in SN 1998S the peak not associated with the CSM torus was observed at zero velocity and attributed to a spherical distribution of shocked CSM clouds. Although a similar solution cannot be invoked to explain a peak centered at -5000 km s^{-1} as seen in SN 2007od, it is possible that this peak comes from the emission of a single cloud or blob of shocked CSM. Since we are seeing the torus and the blob at different velocities, the blob cannot be located in the plane of the torus. At the same time, the blob would be required to have a velocity component along our line of sight larger than that of the torus. Therefore, if the torus is nearly edge on as viewed from Earth (Figure 3.4), as hypothesized in SN 1998S, the blob cannot be moving orthogonal to the plane of the torus as this would severely limit its velocity component along our line of sight. On the other hand, if the inclination[2] of the ring is less than 90°, the blob could be moving orthogonally, but it would require a sufficiently thick torus to retain the dust extinction necessary to explain the asymmetric inner peaks. Without knowing precise mechanisms to create such blobs in the CSM this scenario may appear a bit ad hoc, but it is the one that most closely explains the data.

From days 232 to 699, the relative strength of the emission component at -5000 km s^{-1} is increasing as the inner pair of emission components ($\pm$ 1500 km s^{-1}) slowly disappear. This is likely due to the ejecta moving through, and completely destroying, the torus but not destroying the blob. The underlying broad component is also present at all epochs. The broad component is likely a combination of the residual ejecta emission and, given the flattening of our lightcurve $\sim$10 mag below maximum, a light echo. The contribution to the total broad component by the light echo is expected to grow with time as the ejecta emission fades. Based on the lightcurve, on day 238 the light echo flux would be $\sim$ 20x fainter than the ejecta emission, and on day 348 $\sim$8x fainter than the transmitted ejecta. Therefore the echo should not be a major contributor to the Hα profile at early times, but would be a major contributor of the late-time profile. Figure 3.3 shows the fits to the day 232 and 348 Hα profiles. We have used Gaussians to approximate the intermediate width peaks and a scaled day 50 spectrum to approximate the residual ejecta emission. We should note that the scaled day 50 spectrum is only an approximation to the day 232 and 358 ejecta emission. Realistically, in addition to fading over time, the profile would likely lose its P Cygni absorption, and its overall width would likely decline. The flat-topped profile of the -5000 km s^{-1} component is shown to be well fit by two intermediate width Gaussians possibly due to density enhancements within the CSM cloud or blob. At later times the profile becomes too complex to fit. On days 458 and 672/698, the -5000 km s^{-1} peak begins to dominate and its two component nature becomes more clear. Moreover, there is a continuing fading of the inner peaks to the point where they disappear into the broad emission by day 672/698. As previously mentioned, by this last epoch, the broad emission

[2] $i = 90°$ is edge-on

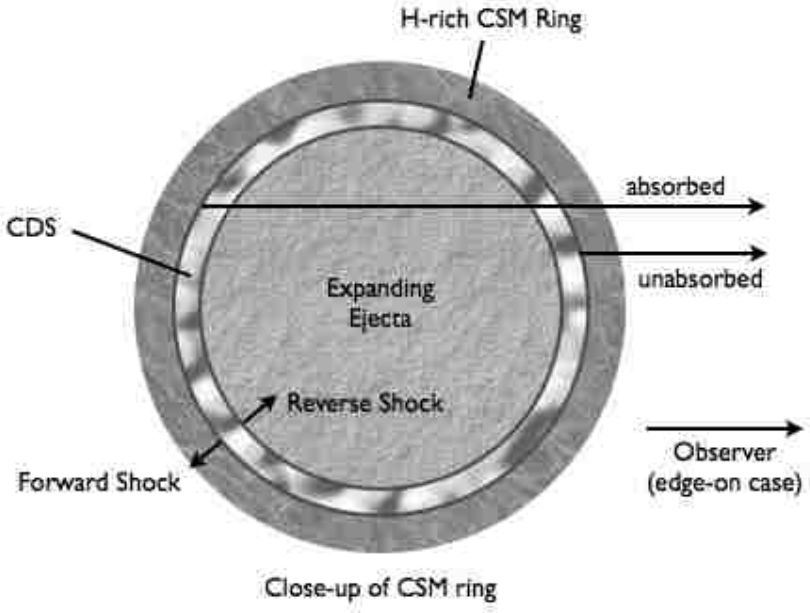

Figure 3.4: A cartoon showing the geometry of SN 2007od (adapted from Mattila et al. (2008) and Fox et al. (2009)). The inner ±1500 km s^{-1} components may come from the forward shock created when the SN ejecta plowed into a central CSM ring, and the outer -5000 km s^{-1} component from the ejecta interacting with a blob of CSM out of the plane of the central ring. If the dust is forming in the CDS between the shocks, then the emission coming from the forward shock at the CSM ring explains why the near-side emission is less reddened than the far-side emission. See text.

is a combination of the light echo spectrum and the weak residual ejecta emission. However, the residual flux beyond 5000 km s^{-1} is unlikely to originate from either of these two sources and remains unexplained. There is also an indication that the radial velocities of both sets of components get smaller with time. This is similar to the behavior of the blue component of SN 1998S which moved to smaller velocities from day 249 to day 658, and was explained as an interaction of the shock with more massive sections of CSM (Pozzo et al., 2004).

3.4 Radiative Transfer Modeling

The SEDs of SN 2007od shown in Figure 3.5 all show strong IR excesses attributable to warm dust. The SED at 300 days can be fitted well by the sum of a blackbody with a temperature of 5100 K representing hot, optically-thick gas in the ejecta and a modified blackbody with a temperature of 580 K subject to a λ^{-1} emissivity law representing the dust. A similar fit to the day 455 SED uses a 5100 K blackbody and a 490 K modified blackbody, and for day 667 a 5100 K blackbody and a 600 K modified blackbody. The fits are shown in Figure 3.5 and the relevant parameters are compiled in Table 3.4. The IR emission could

arise from pre-existing dust in the CSM, and/or new dust condensing in either or both of the CDS and the ejecta itself. IR echoes from pre-existing CSM dust heated by the early-time luminosity are often seen in other SNe. The position of the dust in SN 2007od cannot be inferred from IR observations alone, but when combined with the evidence provided by the asymmetry in the Hα emission components, it suggests that the IR emission is coming from dust forming in the ejecta or the CDS, and not from an IR echo. The very early onset of dust formation (between 114-232 days) further suggests that the dust formation is occurring in the CDS since the ejecta at this time would still be too warm for dust condensation (Kozasa et al., 1991).

Table 3.3: Spitzer Photometry of SN 2007od

Day	3.6μm	4.5μm	5.8μm	8.0μm	16μm	24μm
300	110.1 ± 1.6	156.4 ± 1.8	200.0 ± 7.6	199.5 ± 12.2	-	-
461	37.9 ± 1.4	63.4 ± 1.6	90.0 ± 7.5	122.2 ± 11.8	<59	<35
667	23.5 ± 0.7	33.3 ± 0.8	-	-	-	-

Although no attempts were made to fine tune the models to match the 16 and 24 μm flux upper limits on day ∼455, care was taken to ensure that our preferred model did not predict emitted fluxes that would have been detected given our experimental setup. We found that we were unable to account for this relatively low flux at 16 and 24 μm with compositions dominated by silicate dust (see Figure 3.5). All other parameters being equal, transitioning from amorphous carbon dust to silicate dust has the effect of broadening the IR peak as the SED will then be increased by strong silicate emission features at 10 and 18 μm. These two emission bumps are clearly seen in the Si model in Figure 3.5. The conclusion is that the silicate dominated model predicts too much flux beyond 10 μm at day 455 leading us to favor the amorphous-carbon dominated model with 75% AC and 25% Si. Given this concentration, our best smooth model predicts a total of 1.7 x 10^{-4} $M_\odot$ and 1.9 x 10^{-4} $M_\odot$ of dust on days 300 and 455, respectively, with an increase in τ_v from 1.5 to 2.0 over the two epochs. This implies a total of 2 x 10^{-5} $M_\odot$ of new dust forming between day 300 and 455 after explosion. The values of τ at 6600 Å predicted by our MOCASSIN fits were 1.3 and 1.8 for days 300 and 460, respectively. These opacities are adequate to explain the inner peak height ratios discussed in Section 3.3. Although the constraints were less reliable on the dust mass at day 667, we were able to show that the available data is consistent with our previous epochs with a predicted dust mass of 1.8 x 10^{-4} $M_\odot$ and $\tau_v = 2.75$. The best clumpy model gave a total dust mass of 2.5 x 10^{-4} $M_\odot$ and 4.2 x 10^{-4} $M_\odot$ on days 300 and 455/667, respectively, implying the formation of 1.7 x 10^{-4} $M_\odot$ of new dust formed. In each case, the quantity of dust formed is several orders of magnitude lower than that required to contribute significantly to the dust budget of the early universe (Morgan & Edmunds, 2003).

3.5 Summary

SN 2007od is a very unusual Type IIP SN that shows strong evidence for early-time ($\lesssim$232 days) dust formation in the cool dense shell (CDS) created by the interaction between the ejecta and the circumstellar medium (CSM). Observations prior to day 82 for the optical lightcurve and prior to day 114 for the spectral evolution indicate SN 2007od was a normal Type IIP SN. Photometry and spectra obtained on day 232 revealed that a large post-plateau luminosity drop ($\sim$ 4.5 mag) and the development of multi-peaked Hα emission had

Table 3.4: Blackbody Fits to SN 2007od

	Blackbody Optical			Mod. Blackbody IR			
Epoch	T (K)	R (AU)	L ($L_\odot$)	T (K)	R (AU)	L ($L_\odot$)	$L_{tot.}$ ($L_\odot$)
300 d	5100	5.7	9.2e5	580	1824	2.4e6	3.3e6
455 d	5100	2.9	2.3e5	490	1860	1.1e6	1.3e6
667 d	5100	1.6	7.5e4	600	767	5.1e5	5.8e5

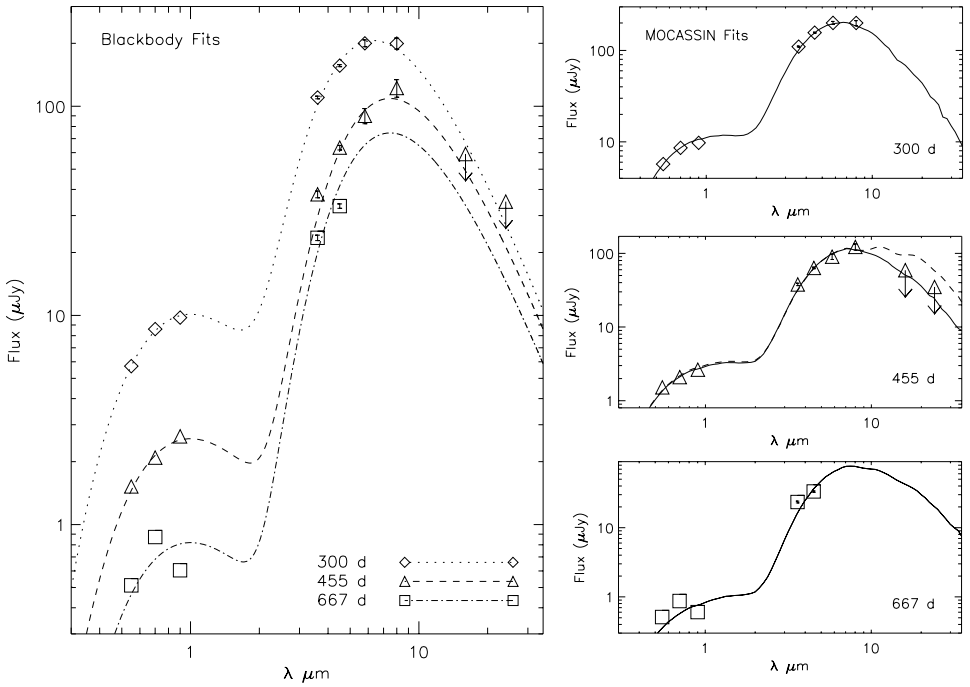

Figure 3.5: SED analysis of SN 2007od on day ∼300 (diamonds), ∼460 (triangles), and ∼667 (squares). Visible wavelengths were obtained with Gemini/GMOS and IR wavelengths with Spitzer/IRAC, IRS PUI, and MIPS. Dust emission is clearly visible in the 3.6-8 μm wavelength range. **Left:** SEDs with best fit blackbody curves. Optical data was fitted with a simple blackbody while the IR data was fitted with a modified blackbody subject to a λ^{-1} emissivity law. **Right:** The corresponding best fit MOCASSIN dust models for each epoch. The best fits reflected a smooth distribution of 75% AC dust (solid lines). For comparison, the best fit 75% silicate model for day 455 (dashed line) is shown and predicts too much flux past 10μm. MOCASSIN input parameters are shown in full in Table 3.5 for each model.

occurred during the period the SN was unobservable. The sharp luminosity decline between days 82 and 232 may have been caused by a low mass ($\lesssim$3 x $10^{-3}M_\odot$) of ^{56}Ni in the ejecta combined with the formation of new dust in the CDS. The presence of dust is supported by the red/blue asymmetries seen in the Hα components as well as the presence of a large IR excess. In SN 2007od, the dust formed between days 114-232 which is much earlier than

Table 3.5: Monte Carlo Radiative Transfer Models of SN 2007od

			Smooth					Clumpy
Epoch	AC/Si	T (K)	R_{in} (AU)	R_{out}(AU)	$L_{tot.}$ ($L_\odot$)	τ_v	M_d ($M_\odot$)	M_d ($M_\odot$)
300 d	0.75/0.25	6000	50.1	2005	3.4e6	1.50	1.7e-4	2.5e-4
455 d	0.75/0.25	6000	50.1	1537	1.4e6	2.00	1.9e-4	4.2e-4
667 d	0.75/0.25	6000	50.1	936	8.1e5	2.75	1.8e-4	4.2e-4

seen for other Type IIP SNe, but in line with SNe that are interacting with the CSM such as SN 1998S. There is also an indication in the late-time photometry that a light echo from surrounding circumstellar or interstellar medium is now being detected.

SN 2007od is unusual in that, while it is classified as a Type IIP, there is evidence for CSM lying close to the progenitor, even though it showed neither a narrow Hα component nor X-ray emission which are both present in typical Type IIn SNe. We believe the multi-peaked Hα emission in SN 2007od is similar to that seen in SN 1998S, and can be explained by the interaction of the ejecta with a circumstellar torus and blob. The $\pm$ 1500 km s^{-1} emission is likely arising from the ejecta interacting with a circumstellar torus, and the -5000 km s^{-1} arises from a single cloud or blob of shocked CSM out of the plane of the CSM.

Our radiative transfer models have indicated that up to 4.2 x $10^{-4}M_\odot$ of dust has formed in the CDS of SN 2007od. The models indicate that 2.5 x $10^{-4}M_\odot$ was present on day 300 and an additional 1.7 x $10^{-4}M_\odot$ formed by day 455. This amount of new dust is similar to estimates for other CCSNe. For example SN 1987A produced 7.5 x 10^{-4} $M_\odot$ of dust (Ercolano et al., 2007) and SN 2006jc an estimated 3 x $10^{-4}M_\odot$ of dust (Mattila et al., 2008). Dust estimates for SN 2003gd currently yield values between 2 x $10^{-4}M_\odot$ and 2 x $10^{-2}M_\odot$ from Sugerman et al. (2006) and 4 x $10^{-5}M_\odot$ from (Meikle et al., 2007), both based on the same data. Monitoring of SN 2007od is continuing in the optical and IR.

4. SN 2007it [3]

SN 2007it was discovered in NGC 5530 by R. Evans visually on 2007 September 13 with V $\sim$ 13.5 mag. (Evans et al., 2007; Itagaki et al., 2007). Pre-discovery images taken with the All Sky Automated Survey (ASAS-3) constrain the explosion date between 2007 September 4-6 (Pojmanski, 2007), and for the purposes of this paper we are assuming an explosion date of 2007 September 5 (JD 2454348). It was confirmed spectroscopically to be a Type II SN by the Carnegie Supernova Project on 2007 September 15 (Contreras et al., 2007). Using Tully et al. (2008), which uses distances set by the 2001 HST Cepheid Key Project observations, we are adopting a distance of 11.7 Mpc throughout this chapter. However it should be noted that a previous study done by Tully (1988) had suggested a distance of 16.9 Mpc. We have obtained visible spectroscopy and photometry as well as mid-IR photometry of SN 2007it spanning days 107-944. Lists of these observations are presented in Tables 4.1 and 4.2. In this chapter, we follow the evolution of the Type IIP SN 2007it in the optical and IR from day 10 to day 944. This makes SN 2007it one of only a few Type IIP SNe with long-term and extensive spectral and photometric observations, along with SN 1990E, SN 1999em, SN 1999gi, SN 2002hh, SN 2003gd, SN 2004et, and SN 2005cs (Maguire et al., 2010, and references therein).

4.1 Lightcurve Evolution

4.1.1 Day 9 - Day 339

The photometric evolution of SN 2007it at early times seems to be consistent with other Type IIP supernova lightcurves, as can be seen in Figure 4.1. The magnitudes are listed in Table 4.3. The plateau phase appears to begin near day 20, and lasts until around the time that the SN becomes visible again on day 107 when it is in midst of its the post-plateau drop in brightness. Therefore the plateau phase lasted $\sim$ 80 days. Given the distance to SN 2007it and the V magnitudes on day 20 and day 107, the average absolute magnitude of SN 2007it on day $\sim$50 is estimated to be M_V=-16.7 (L = 1.6 $\times$ 10^{42} erg s^{-1}), once corrections for reddening have been made. Comparing these values with other Type IIP SNe (Maguire et al., 2010, and references therein) indicates that SN 2007it is one of the more luminous, well studied Type IIP SNe to date and is quite similar to SN 2004et (see Figure 4.2).

After the plateau phase, the drop to the radioactive tail is roughly 2 mag. Type IIP SN normally experience a decrease in luminosity of $\sim$1.5-3 mag based upon the amount of ^{56}Ni present (Woosley & Weaver, 1986; Kasen & Woosley, 2009). For comparison, SN 2007it shows roughly the same plateau duration and drop as SN 2004et (Figure 4.2), which may suggest a similar ^{56}Ni mass. This is discussed in more detail below. The decline in luminosity then follows the ^{56}Co decay closely (see Figure 4.1), until the SN is lost behind the sun after day 339.

4.1.2 Day 509 - Day 922

Once SN 2007it was observed again on day 509, we found that its brightness had fallen below the expected ^{56}Co decay by $\sim$ 0.5 mag in R. The R band contains the Hα and [O I]

[3] Andrews et al. (2011)

Table 4.1: Photometry Summary of SN 2007it

Day	JD	Telescope	Instrument	Exposures	Exposure Time *(s)*
107	2454455	SMARTS 1.3m	ANDICAM	5	20
113	2454461	SMARTS 1.3m	ANDICAM	5	20
139	2454487	SMARTS 1.3m	ANDICAM	5	20
157	2454505	SMARTS 1.3m	ANDICAM	5	20
188	2454536	SMARTS 1.3m	ANDICAM	5	20
209	2454557	Gemini South	GMOS Imaging	3	20
223	2454571	SMARTS 1.3m	ANDICAM	5	20
242	2454590	Gemini South	GMOS Imaging	3	20
252	2454600	SMARTS 1.3m	ANDICAM	3	100
276	2454624	SMARTS 1.3m	ANDICAM	3	100
279	2454627	Gemini South	GMOS Imaging	3	20
300	2454648	SMARTS 1.3m	ANDICAM	3	100
302	2454650	Gemini South	GMOS Imaging	3	20
314	2454662	SMARTS 1.3m	ANDICAM	3	100
339	2454687	Gemini South	GMOS Imaging	3	20
351	2454699	Spitzer	IRAC	12	100
540	2454888	Gemini South	GMOS Imaging	1	60
561	2454909	Spitzer	IRAC	12	100
566	2454914	Gemini South	GMOS Imaging	2	60
589	2454937	Gemini South	GMOS Imaging	2	60
613	2454961	HST	WFPC2	4	412
622	2454970	Gemini South	GMOS Imaging	2	60
696	2455044	HST	ACS/WFC	4	412
718	2455066	Spitzer	IRAC	12	100
916	2455264	Gemini South	GMOS Imaging	2	60
922	2455270	HST	ACS/WFC	4	424

Table 4.2: Spectroscopy Summary of SN 2007it

Day	JD	Telescope	Instrument	Exposures	Exposure Time *(s)*
154	2454502	Gemini South	GMOS Spectra	3	900
178	2454526	Gemini South	GMOS Spectra	3	900
209	2454557	Gemini South	GMOS Spectra	3	900
242	2454590	Gemini South	GMOS Spectra	3	900
279	2454627	Gemini South	GMOS Spectra	3	900
302	2454650	Gemini South	GMOS Spectra	3	900
339	2454687	Gemini South	GMOS Spectra	3	900
540	2454888	Gemini South	GMOS Spectra	3	1800
566	2454914	Gemini South	GMOS Spectra	3	1800
589	2454937	Gemini South	GMOS Spectra	3	1800
622	2454970	Gemini South	GMOS Spectra	3	1800
916	2455264	Gemini South	GMOS Spectra	3	1800

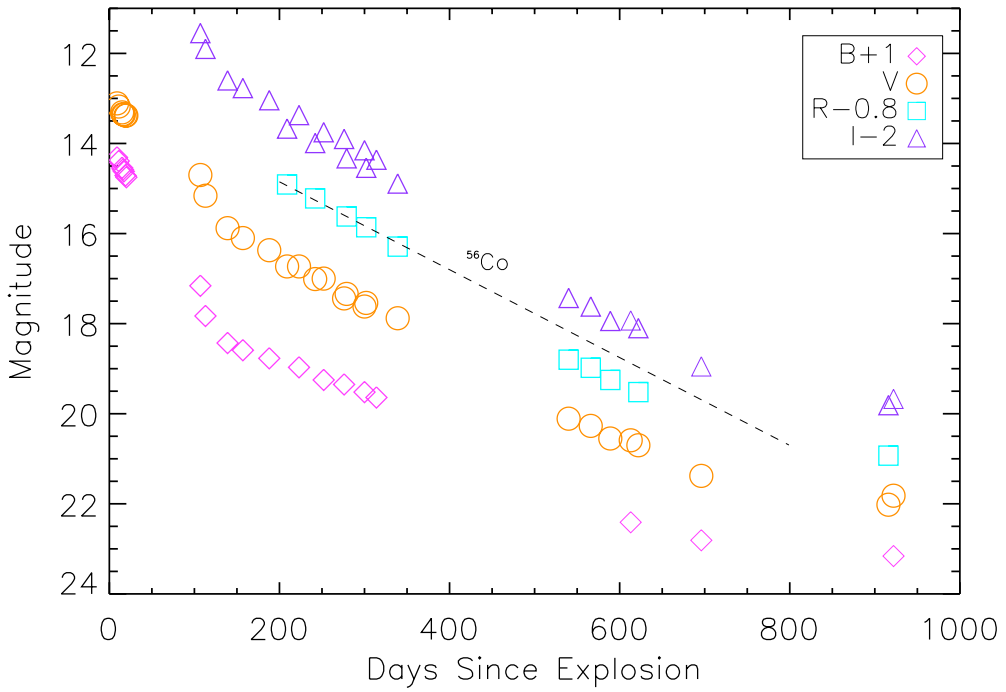

Figure 4.1: Optical BVRI lightcurves of SN 2007it. Photometry before day 100 was obtained from Carnegie Supernova Project. The disagreement in values in I between days 200 and 400 is likely due to bandpass differences between SMARTS and Gemini filters.

Table 4.3: Optical Photometry of SN 2007it

Day	B	V	R	I
107	16.16 ±0.10	14.70 ± 0.04	-	13.55 ±0.04
113	16.83 ±0.11	15.16 ± 0.08	-	13.90 ± 0.06
139	17.43 ±0.04	15.88 ± 0.03	-	14.60 ± 0.03
157	17.59 ±0.04	16.1 ± 0.03	-	14.77 ± 0.03
188	17.77 ±0.05	16.37± 0.02	-	15.04 ± 0.03
209	-	16.73± 0.04	15.71 ±0.03	15.67 ± 0.03
223	17.97 ±0.03	16.73 ± 0.03	-	15.37 ± 0.03
242	-	17.01 ± 0.04	16.02 ± 0.02	15.99 ± 0.03
252	18.52 ±0.05	17.00 ± 0.03	-	15.75± 0.09
276	18.35 ±0.04	17.23 ± 0.03	-	15.90 ± 0.03
279	-	17.34 ± 0.04	16.42 ± 0.02	16.33 ± 0.03
300	18.52 ±0.05	17.44 ± 0.03	-	16.15 ± 0.03
302	-	17.54 ± 0.04	16.66 ± 0.03	16.54 ± 0.02
314	18.64 ±0.05	17.62 ± 0.05	-	16.36 ± 0.04
339	-	17.88 ± 0.04	17.09 ± 0.04	16.89 ± 0.05
540	-	20.11 ± 0.04	19.60 ± 0.03	19.43± 0.03
566	-	20.27 ± 0.04	19.78 ± 0.04	19.62 ± 0.05
589	-	20.55 ± 0.04	20.05 ± 0.02	19.94± 0.03
613	21.41 ±0.16	20.59±0.11	-	19.93 ±0.09
622	-	20.7 ± 0.04	20.32 ± 0.03	20.10 ± 0.03
696	21.81 ±0.12	21.38 ±0.05	-	20.95 ±0.05
916	-	22.02 ±0.03	21.73 ±0.03	21.81 ±0.04
922	22.16 ±0.18	21.82 ±0.10	-	20.95 ±0.14

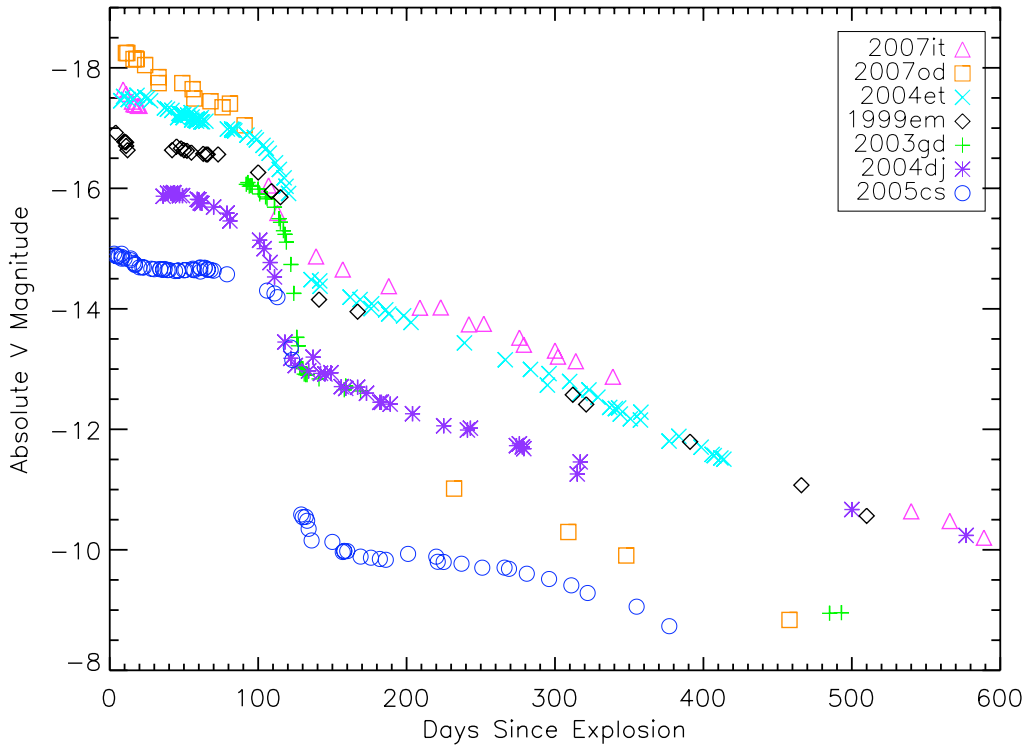

Figure 4.2: Absolute V light curves of a sample of Type IIP SNe. All SNe have been corrected for reddening and the data are from: SN 2007od (Andrews et al., 2010), SN 2004et (Kotak et al., 2009; Misra et al., 2007), SN 1999em (Elmhamdi et al., 2003b), SN 2003gd (Hendry et al., 2005), SN 2004dj (Vinkó et al., 2006; Zhang et al., 2006), and SN 2005cs (Pastorello et al., 2009).

$\lambda\lambda$ 6300,6364 Å emission features, which are responsible for most of the flux at late times. The most likely cause for this decreased decline in brightness is new dust formation between days 339 and 509. This is the time period during which dust typically condenses in the ejecta of SNe. After this drop, the ^{56}Co decay was maintained, indicating that little or no further dust formation occurred after day 509. Other dust indicators such as the simultaneous increase in the IR luminosity and red-wing attenuation of the [O I] lines, discussed below, indicate that this is indeed the case.

Also of note is another deviation from the ^{56}Co decay curve seen as a flattening of the lightcurve after day 700. This was also seen in SN 2007od (discussed in Chapter 3), SN 2003gd (Sugerman, 2005), and SN 2002hh (Welch et al., 2007), and is likely a light echo caused by dust reflecting light from the flash of the SN explosion, keeping the luminosity brighter than expected at late times. Scattered light echoes are expected to become major contributors to the emission of SNe around 8-9 mag below maximum (Patat, 2005), which is when we see the flattening of the SN 2007it lightcurve. Analysis of this echo is beyond the scope of this thesis, and will be presented in a forthcoming paper. Subtraction of images of SN 2007it taken with HST/ACS on day 922 and WFC3 between days 857 and 1009 (to presented in another paper) seen in Figure 4.3 revealed a residual in the southwest corner

roughly 4 pixels from the center of the SN corresponding to an echo from ISM material ∼21 pc away from the SN (Andrews et al. 2011, in preparation). Comparison of photometry from early times to the late-time flattening, show the late-time color is much bluer, with B-V dropping from ∼1.5 on day 107, to ∼ 0.3 on day 922. This will happen when the CSM or ISM dust is preferentially scattering the blue light as was seen in SN 2006gy on day 810 (Miller et al., 2010). The resolved light echo, along with the blue late-time colors, indicate that the flattening of the light curve after day 696 is likely due to a light echo and not CSM interaction at late times.

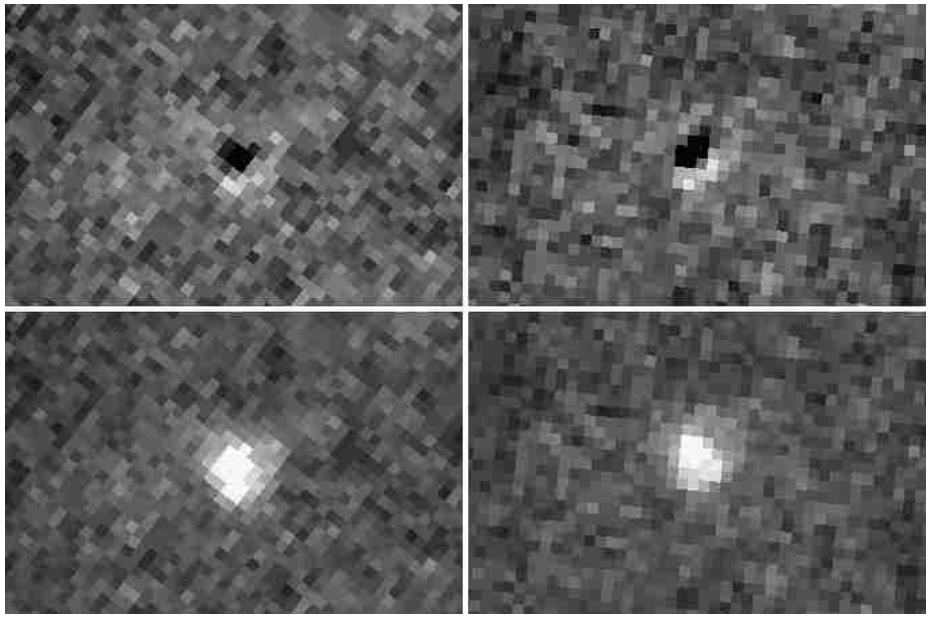

Figure 4.3: Bottom panels show HST/WFC3 F814W images of SN 2007it from day 857 (left) and 921 (right), while the top panels show a PSF-subtracted image of the SN. The residual material, shown as white pixels to the lower-right of the subtracted SN is the light echo material which is ∼ 21 pc away from the SN.

4.2 Spectral Evolution

Figure 4.4 shows the optical spectral evolution of SN 2007it from day 10 to day 922. The early time spectra show broad Hα and Hβ emission and strong Na I D absorption. The Hα evolution is seen in Figure 4.5, and shows a blueshift for at least the first 200 days. Blueshifted Hα emission has been seen in other Type II SNe such as SN 1988A (Turatto et al., 1993a), SN 1998A (Pastorello et al., 2005), and SN 1999em (Elmhamdi et al., 2003b). Chugai (1988b) and later Jeffery & Branch (1990) proposed that this was caused by the reflection of photons by the photosphere. For 1988A and 1999em, the blueshift only lasted ∼80 days, whereas SN 2007it and SN 1998A seem to have a blueshift persisting well past 150 days. By day 200, when the SN is well into the nebular phase, strong [O I] $\lambda\lambda$ 6300,6363 Å emission is seen (shown in Figure 4.4), as well as [Ca II] $\lambda\lambda$7291,7324 and [Fe II] λ7155 Å emission.

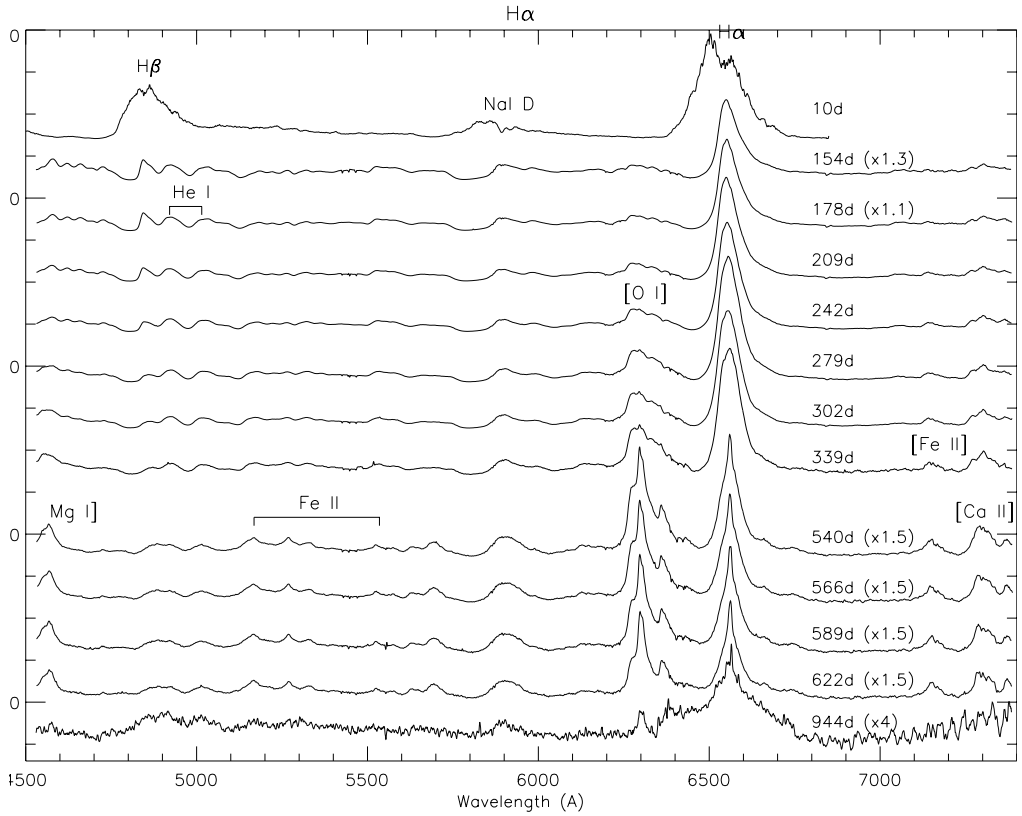

Figure 4.4: Spectral evolution of SN 2007it from day 10 to day 922. All spectra other than day 10 are from Gemini/GMOS. Of interest is the brightness of the [O I] $\lambda\lambda$ 6300,6363 lines in relation to Hα and [Ca II] lines.

Once we recover SN 2007it at day 509, the [O I] line strengths rival that of Hα, while the [Ca II] lines are at most, half the strength of Hα. This is unusual for Type IIP SNe, since most exhibit stronger [Ca II] than [O I]. The only other example of a Type II SN with similar late-time line strengths as SN 2007it, was the Type IIL SN 1970G (Pronik et al., 1976; Chugai, 1988a). Unfortunately no optical spectra were taken after $\sim$ day 350 of SN 1970G to allow further comparisons of the spectral evolution. There is also an emission feature emerging after day 200 at 7380 Å which is separate from the [Ca II]/[O II] blended lines, and could be a [Ni II] λ7380 Å line which was also identified in the Type IIn SN 2006gy (Kawabata et al., 2009), Type Ic SN 2006aj (Maeda et al., 2007), and a few type Ia SNe (Maeda et al., 2010). This line may be present in other SNe but hidden by strong [Ca II] emission (Maeda et al., 2007).

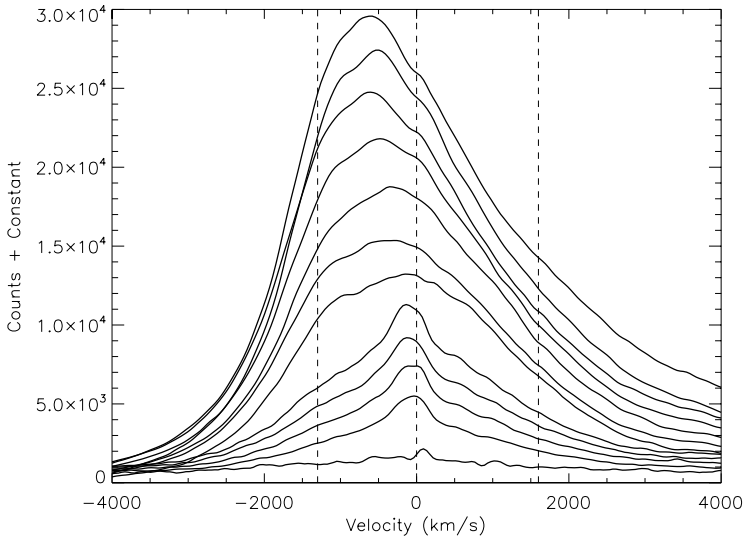

Figure 4.5: Hα evolution from day 154 (top) to day 922 (bottom). Notice the emergence of an intermediate width component starting on day 540 which may indicate CSM interaction. The blue-shift of the intermediate peak is due to newly formed dust attenuating the red side more than the blue.

Of special note are the multi-component peaks of the [O I] $\lambda\lambda$6300,6364 Å lines that are visible in our day 154 spectra and persist to day 622 (Figure 4.6). These emission line profiles are similar to the multiple peaks seen in the Hα emission of SNe 1998S (Leonard et al., 2000) and 2007od (Chapter 3). Both the 6300 and 6364 Å lines have a blue-shifted component occurring at -1300 km s^{-1} in relation to the component seen at the rest velocity of the galaxy. There seems to be no corresponding red peak at +1300 km s^{-1}. Because CSM interaction is normally only seen in H and He lines, this suggests another origin for the multiple peaks. Similar asymmetries in the [O I] lines have been seen in numerous H-poor CCSNe (Type Ib, Ic, and IIb), for example SNe 2005aj, 2006T, and 2008ax, but seems to be rare in normal Type IIP (Modjaz et al., 2008; Taubenberger et al., 2009; Milisavljevic et al., 2010). These asymmetries can be seen approximately 2 months post explosion in H-poor CCSNe, but due to the lack of spectral observations between days 10 and 154 in

SN 2007it, we cannot pinpoint the exact date before day 154 when the [O I] lines and the corresponding asymmetries appeared. Milisavljevic et al. (2010) suggest that the the absence of a red component combined with the presence of a blue peak the same distance away from both the 6300 Å and 6364 Å lines could be explained by emission from an asymmetric blob of O material ejected on the forward side of the SN during the explosion. They do caution that a torus of O material is less likely but cannot be ruled out, and that the red-shifted components could exist but are hidden either by the SN orientation or obscuring dust. The existence of fast moving knots seen in oxygen-rich SN remnants such as Puppis A and Cas A may substantiate the asymmetric blob scenario. According to Winkler & Kirshner (1985), it is likely that these knots are intact fragments of the core of the progenitor star. These remnant oxygen knots have radial velocities consistent with the blue [O I] components of SN 2007it.

Signatures of CSM interaction can also be seen in the Hα and [O I] lines (Figures 4.5 and 4.6). The CSM interaction is manifested as a narrower feature (FWHM $\sim$ 1000 km s^{-1}) at the rest velocity rising above the broader (FWHM $\sim$4000 km s^{-1}) ejecta base. Although this feature does not become apparent until day 509 in the Hα spectra, it seems to be present since day 154 in the [O I] emission. We then surmise that the intermediate peak was present in both lines since day 154, but the overwhelming ejecta emission in Hα kept it hidden until day 509. From the day 154 spectra and onward in [O I] there also seems to be an attenuation of the red-wing of the central peak, especially in 6300 Å which becomes even more apparent after day 509 when the asymmetric blob emission has faded. There are two possibilities for these asymmetries, attenuation from pre-existing dust or Bochum events like that seen in Hα of SNe 1987A and 1999em. Bochum events are the emergence of two peaks in the Hα profile, usually at early times, due to asymmetric ^{56}Ni ejection, which will cause an asymmetric ionization. For a full discussion on these events see Elmhamdi et al. (2003b). The shape of the [O I] central peaks are similar to modeled profiles presented in Elmhamdi et al. (2003b), where the peak has been shifted toward the blue side due to the presence of dust in the ejecta. As we will show below, IR data from day 351 suggests the presence of an IR echo from flash-heated pre-existing dust. This pre-existing dust is likely the cause of the attenuation seen in the [O I] lines. We do not see signatures of new dust forming from asymmetries in the spectral lines, although we must point out that it is possible that if the new dust is concentrated in a ring or torus around the SN, newly formed dust could be hidden by the viewing angle.

4.2.1 Mass estimates

We estimate a ^{56}Ni mass for SN 2007it of M_{Ni}= $0.09^{+.01}_{-.02}$ $M_\odot$ from the methods of Hamuy (2003). The bolometric luminosity of the radioactive tail (in erg s^{-1}) is calculated as

$$\log_{10} L_t = \frac{-[V_t - A(V) + BC] + 5\log_{10} D - 8.14}{2.5}, \tag{4.1}$$

with A_V = 0.39 mag, and a bolometric correction of BC = 0.26. The nickel mass is then calculated at various times during this phase, as

$$M_{Ni} = (7.866 \times 10^{-44}) L_t \exp\left[\frac{\frac{t_t - t_0}{1+z} - 6.1}{111.26}\right] M_\odot. \tag{4.2}$$

Here 6.1 and 111.26 days are the half-lives of ^{56}Ni and ^{56}Co, respectively, and t_t-t_0 is the age of the SN. This calculated Ni mass is similar, if slightly higher, than other Type IIP SNe. SN

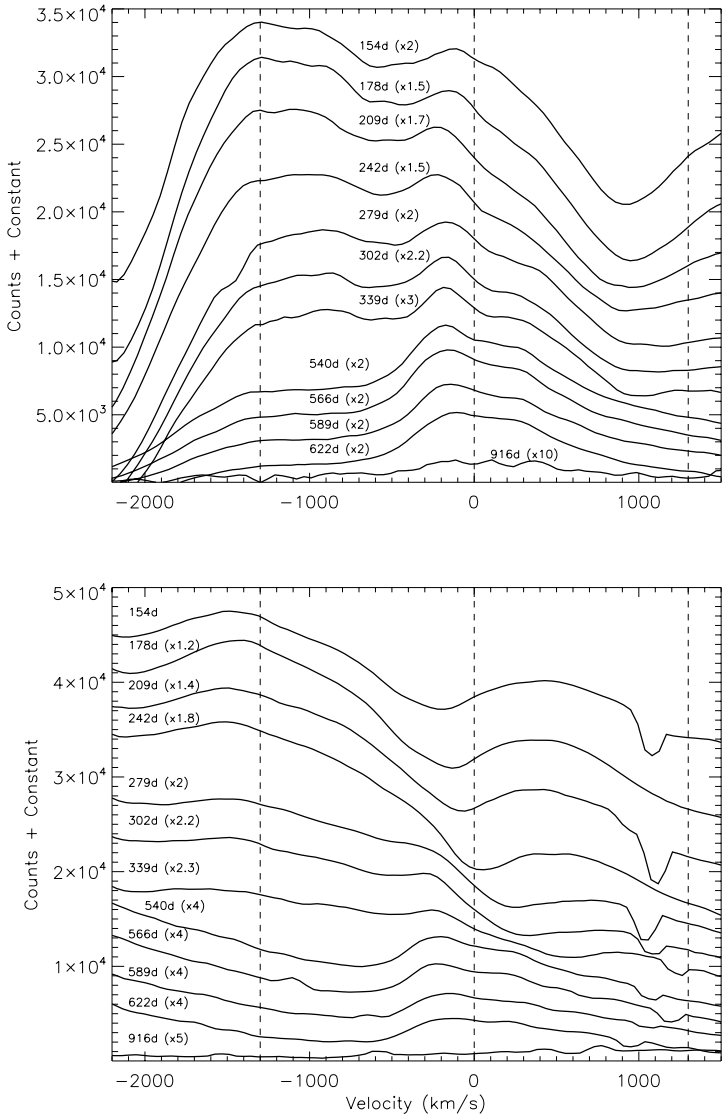

Figure 4.6: Evolution of [O I] λ6300 Å (top) and λ 6364 Å lines from day 154 to day 922. There is a separate blue-shifted component at -1300 km s^{-1} from each [O I] line, which we believe is created by a blob of O-rich ejecta on the forward side of the SN.

2004et has an estimated M_{Ni} mass of 0.056 $M_\odot$(Maguire et al., 2010). SNe 1999em, 2003gd, and 2004dj each have ∼0.02 $M_\odot$ (Elmhamdi et al., 2003b; Hendry et al., 2005; Vinkó et al., 2006), and the low-luminosity SN 2005cs contains 3 x $10^{-3}M_\odot$ of ^{56}Ni (Pastorello et al., 2009).

We have estimated the mass of oxygen two separate ways using the strength of the [O I] doublet in the nebular phase before the onset of dust formation. Using a temperature range of 3500-4000 K, and a flux ($F_{[OI]}$) of 9.7 × 10^{-14} erg s^{-1} cm^{-2} for the day 286 spectrum

(obtained from the Carnegie Supernova Project) we estimate M_O= 0.2-0.9 $M_\odot$ using

$$M_{[OI]} = 10^8 F_{[OI]} D^2 e^{2.28/T_4} \tag{4.3}$$

which is Equation 1 in Uomoto (1986). Where T_4 is the temperature in 10^4 K, and D is the distance in cm. As a second method we implemented the relationship given in Elmhamdi et al. (2003b),

$$L_{[OI]} = \eta \frac{M_O}{M_{exc}} L_{Co} \tag{4.4}$$

under the assumption that SN 2007it had the same η (the efficiency of energy transfer from O mass to [O I] doublet luminosity) and excited mass as SN 1987A, and that the L_{Co}, the luminosity of the Co emission, was directly related to the mass of ^{56}Ni. Once again we used an oxygen flux of 9.7×10^{-14} erg s^{-1} cm^{-2}. This calculation gives us an oxygen mass of 0.96 that of SN 1987A, or between 1.15-1.44 $M_\odot$. These values, although not consistent with each other, are very similar to the values calculated for SN 2004et in Maguire et al. (2010).

Comparing the relationship between ^{56}Ni and progenitor mass in other SNe (for example, Table 5 in Misra et al. (2007)), it is likely that SN 2007it had a main sequence mass $\geq$ 20 $M_\odot$. Recently, Dessart et al. (2010) have suggested that using the velocity of the Hα line at $\sim$ day 15 and the velocity of the [O I] $\lambda\lambda$ 6300,6363 Å lines at $\sim$ 300 days could be an indicator of progenitor ZAMS mass. Using the values of 10960 km s^{-1} and 2000 km s^{-1}, respectively, and the estimated mass of oxygen calculation above suggests a progenitor mass between 16-20 $M_\odot$. Fransson & Chevalier (1987, 1989) have also suggested that the ratio between [Ca II]/[O I] lines in the nebular phase can be an indicator of progenitor mass, with smaller ratios belonging to higher mass progenitors. This ratio is 0.7 for SN 2007it between days 209-351, which is quite small for a Type IIP SN. Elmhamdi et al. (2004) showed that SN with ratios similar to SN 2007it are normally of Type Ib/c. SN 1987A had a ratio of $\sim$ 3 from day 250-450 and SN 2005cs meanwhile showed a ratio of 4.2 $\pm$0.6 on day 334 (Pastorello et al., 2009), which is 40% larger than SN 1987A, and over 6 times greater than SN 2007it. This may indicate that the progenitor of SN 2007it may have been more massive than either SN 2005cs (7-13 $M_\odot$) and SN 1987A (14-20 $M_\odot$), with a mass of roughly 20-27 $M_\odot$. All of these estimates suggest that SN 2007it had a progenitor mass of $\sim 20^{+7}_{-4} M_\odot$. Unfortunately, no images of the progenitor star exist.

4.3 Mid-IR Evolution

SN 2007it was monitored in the mid-IR for four epochs spanning days 351- 944 (see Table 4.4). As can be seen in Figure 4.7, the first epoch on day 351 shows an indication of an increased flux in the 4.5 μm band with respect to the other channels. This elevated emission in this band photometry was also seen around the same time period in SNe 2005af (Kotak et al., 2006), 2004dj (Kotak et al., 2005) and 2004et (Kotak et al., 2009), and has been attributed to CO fundamental band emission. Less prominent is the possible extra emission at 8.0 μm which may be due to SiO emission. SiO emission was discovered in 1987A (Roche et al., 1991) and also in SN 2004et (Kotak et al., 2009), and 2005af (Kotak et al., 2006). CO and SiO are thought to be precursors to dust formation (Nozawa et al., 2003) since they likely provide the molecular foundation from which the dust grains form. Therefore the presence of these molecules is important in understanding the whole story of dust formation in SNe.

Table 4.4: Spitzer Photometry of SN 2007it

Day	3.6μm (μJy)	4.5μm (μJy)	5.8μm (μJy)	8.0μm (μJy)
351	257.28 ± 6.64	625.75 ± 12.10	317.40 ± 13.16	363.41 ± 23.28
561	528.69 ± 11.69	600.90 ± 11.07	660.69 ± 17.65	628.06 ± 23.14
718	213.21 ± 6.11	354.16 ± 7.15	-	-
944	39.12 ± 2.30	142.96 ± 3.28	-	-

Day 351 shows the presence of an IR excess, well before the estimated time of new dust formation as indicated by visible photometry. A likely cause for this elevated flux is an IR echo from flash-heated pre-existing CSM dust. Using the optical spectra on day 339 before the CSM interaction is apparent in Hα and day 540 when the intermediate peak is visible along with the fastest ejecta velocity on day 10 of 10 900 km s^{-1}, we can estimate that the initial SN flash has cleared a dust-free cavity between 3.2 and 5.3 x 10^{16} cm from the center. This agrees with estimates for SN 2005ip, which has the same estimated $L_{peak} \sim 10^9$ $L_\odot$, and a vaporization radius of $\sim 10^{16}$ cm (Fox et al., 2010). Assuming a cavity was cleared out to 4 x 10^{16} cm, the optical and UV light would reach this boundary at around 15 days. We do not have any IR observations prior to day 351, so we cannot definitively suggest the early behavior, but it is likely that an IR excess was present early on and we are seeing the continued plateau of this heated dust on day 351. Models by Dwek (1985) indicate that a combination carbon and oxygen rich shell could very likely produce a plateau of this length, thereby creating the IR excess seen on this first epoch.

The IR fluxes on day 561 are very different from day 351, most importantly the fluxes in the 3.6, 5.8 and 8.0 μm channels have doubled in intensity. This may indicate that new dust grains have formed. This is likely since this is the same time period in which we see a dimming in the visible lightcurve (between days 339 and 540). The combination of the elevated mid-IR flux at the same time as the corresponding dimming in the visible can be explained if dust grains are absorbing the high energy photons and re-emitting them in the IR. This has been seen in other dust producing CCSNe such as SN 1987A (Suntzeff et al., 1991) and SN 2003gd (Sugerman et al., 2006). Modified blackbody fits to this epoch indicate a blackbody luminosity of 4.5 x 10^{38} erg s^{-1}, twice the blackbody luminosity at day 351. This is consistent with the optical drop of 0.5 mag, which is equal to a drop of 1.58 in luminosity. Within the uncertainties, the drop in optical luminosity is equal to the increase in IR luminosity.

Days 718 and 922 were both observed by Spitzer in warm mode, so only the 3.6 and 4.5 μm bands were available. Both epochs show significant IR luminosity, likely due to the newly formed ejecta dust. In the day 922 data, the 4.5 μm flux appears to be stronger than expected, and in fact the ratio between 3.6 and 4.5 is much smaller than other epochs, only 0.27 as opposed to 0.6 on day 718. If we assume the ratio to be constant in the day 922 epoch, we would expect a flux of $\sim$ 66 μJy, but instead see a flux of 143 μJy, indicating that there is possibly an excess in the 4.5 μm channel. This is also seen by Sugerman et al. (2011, in preparation) for SN 2004et. It is likely we are still seeing CO emission that was visible on day 351, which was hidden by the increased emission from the new dust on day 561, and became visible again in the later epochs as the grains cooled.

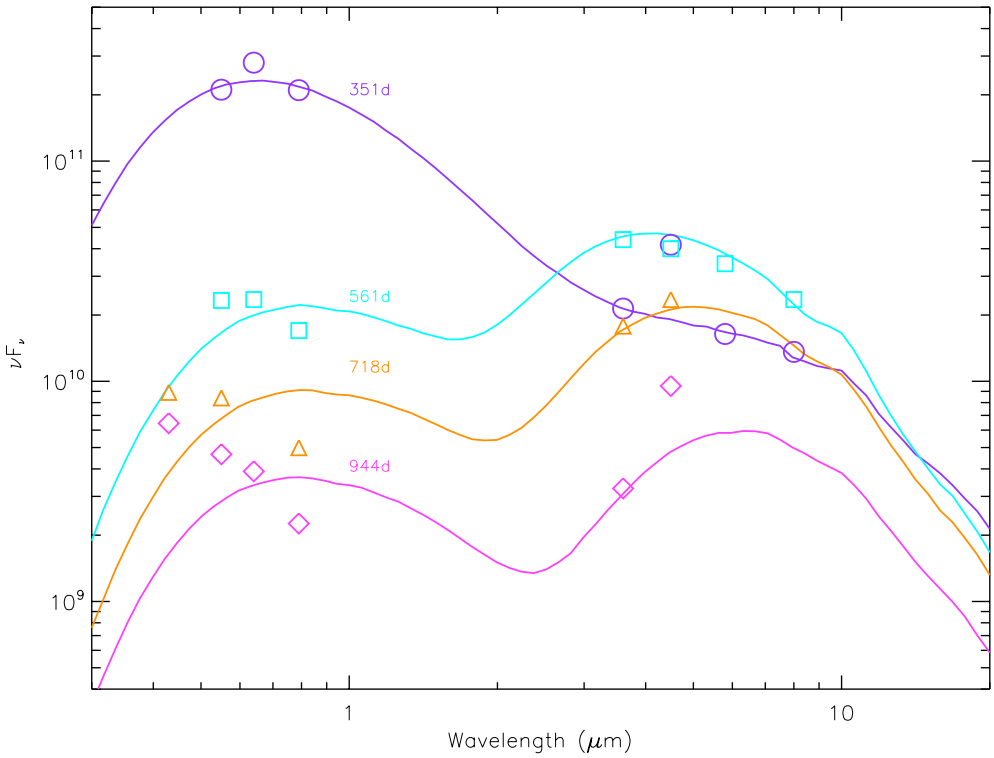

Figure 4.7: MOCASSIN fits from our smooth shell modeling scenario (Table 4.5) for days 351 (circles), 561 (squares), 718 (triangles), and 944 (diamonds). The optical points are from day 339, 566, 696, and 916 (Table 4.3), and have been corrected for foreground extinction. Error bars are equal to or smaller than symbol size. On days 718 and 944 a large portion of the optical luminosity is likely derived from the light echo, which due to its scattering nature will make the SN appear to be more blue (Patat, 2005). The clumpy shell and torus modeling is consistent with the smooth shell fits, and are not shown.

4.4 Radiative Transfer Modeling

As we assumed for SN 2007od (Chapter 3), in these models the dust and luminosity for the source was located between inner radius R_{in} and outer radius R_{out} of a spherically expanding shell, with the luminosity being proportional to the density at each location. For day 351 we have chosen to concentrate the luminosity in a point source, rather than spread throughout the shell, as it is likely this emission is the result of flash-heated pre-existing CSM. This does create a better fit to the IR data points.

For each model we used a combination of amorphous carbon (AC) and silicate grains, using the optical constants of Hanner (1988) and Draine & Lee (1984), respectively. For all epochs the best fit occurred with a carbon rich combination of 75% AC and 25% silicates, as was also the case in SN 2007od (Chapter 3). For day 351 no attempt was made to fit the 4.5 μm point, since it was likely due mainly to CO emission, the same is true for day 922 when CO may also be responsible for the elevated 4.5 μm flux.

Initial estimates for each input parameter were accomplished using black body fits to the optical and IR data. This yielded dust temperatures of roughly 500 K for the first epoch, and 700K for the remaining epochs. These temperatures are consistent with typical warm dust temperatures. For our first epoch, we used an R_{in} of 3.2 x 10^{16} cm, which roughly corresponds to the evaporation radius of the initial flash of the SN. All other epochs used an R_{in} of 7 x 10^{15} cm which created the best fits. We also kept T = 5700K for all epochs, since this is a reasonable ejecta temperature and does an adequate job fitting the first epoch of optical points. The combination of high Hα flux and [O I] emission lines in the R band relative to the continuum, and at later times additional flux due to the light echo has made it unlikely that the visible photometry is consistent with any reasonable blackbody temperature. Keeping those two values constant, we then varied the luminosity, outer radii, and dust masses to get the most accurate fits. For all epochs we found that the clumpy distribution predicted on average slightly higher dust masses than the smooth and torus models.

We estimate a dust mass for our first epoch of 5 x $10^{-4} M_{\odot}$ for the smooth model, 7.3 x $10^{-4} M_{\odot}$ for clumpy, and 1.6 x $10^{-4} M_{\odot}$ for the torus. The remaining epochs yielded smooth dust masses of 7.0 x $10^{-5} M_{\odot}$ for day 561, 8.0 x $10^{-5} M_{\odot}$ for day 718, and 4.6 x $10^{-5} M_{\odot}$ for day 922. The larger dust mass from the first epoch might be explained by the flash heating of pre-exisiting CSM dust in an area much further away and roughly 200K cooler than following epochs. At this first epoch R_{in} = 3.2 x 10^{16} cm, which is larger than the R_{out} of the remaining epochs. This pre-existing dust will cool, as described in Section 4.3 above, and fade after its initial heating by the SN flash so that by day 561 the IR SED is dominated by newly formed ejecta dust. After day 561, R_{in} = 7 x 10^{15} and R_{out} = 2 x 10^{16}, which likely places the dust at this time in the CDS interior to the point of CSM interaction. These results also indicate that the amount of new dust created is smaller than the amount in the CSM.

On day 351,the MOCASSIN models estimate that $\tau_v = 0.08$. In order to independently estimate the optical depth, we used the methods of Fox et al. (2009) which uses total peak energy and IR energy($\tau \sim \frac{E_{IR}}{E_{IR}+E}$). The peak luminosity of SN 2007it was $\sim 10^9$ $L_{\odot}$, which would indicate E $\sim 10^{49}$ erg using the estimates of SN 2005ip contained in Fox et al. (2009). The IR energy for the first 351 days is then 1 x 10^{48} erg, using an L_{bb} of 8.8 x 10^6 $L_{\odot}$. This yields a $\tau = 0.09$, consistent with our MOCASSIN fits. Between day 351 and 561 we also find a significant increase in τ_v, which jumps from 0.08 to 1.27 as the new dust forms. This is largely due to the order of magnitude decrease in R_{out} between the two epochs, requiring similar amounts of dust in a much smaller volume. Although the optical light curve suggests only an $A_V = 0.5$, considerations of geometry, such as the newly formed dust existing in a torus around the SN for which we are seeing inclined at an angle away from edge-on, could explain the higher amount estimated from MOCCASIN which would provide the total optical depth summed over the whole system, not just along our line of sight. This scenario could also explain the lack of increased attenuation in the [O I] and Hα spectral lines between days 339 and 540 when we see the other dust formation signatures, mainly the simultaneous increase in optical extinction and IR luminosity. Therefore the total mass of new dust formed in SN 2007it appears to be $\sim$ 1.0 x $10^{-4} M_{\odot}$, which although consistent with dust masses of other CCSNe, is still considerably smaller than the amount needed to account for the dust seen at high-z (Morgan & Edmunds, 2003).

Table 4.5: Smooth and Clumpy Monte Carlo Radiative Transfer Models of SN 2007it

Epoch	AC/Si	T (K)	R_{in} (cm)	R_{out}(cm)	$L_{tot.}$ ($L_\odot$)	τ_v	Smooth M_d ($M_\odot$)	Clumpy M_d ($M_\odot$)
351 d	0.75/0.25	5700	3.2e16	9.0e17	1.9e7	0.08	5.0e-4	7.3e-4
561 d	0.75/0.25	5700	7.0e15	2.0e16	4.6e6	1.29	7.0e-5	1.0e-4
718 d	0.75/0.25	5700	7.0e15	2.0e16	2.4e6	1.4	8.0e-5	1.3e-4
944 d	0.75/0.25	5700	7.0e15	2.0e16	6.9e5	0.98	4.6e-5	1.3e-4

Table 4.6: Monte Carlo Radiative Transfer Torus Models of SN 2007it

Epoch	AC/Si	T (K)	R_{in} (cm)	R_{out}(cm)	$L_{tot.}$ ($L_\odot$)	τ_v	M_d ($M_\odot$)
351 d	0.75/0.25	5700	3.2e16	2.5e17	1.9e7	0.08	1.6e-4
561 d	0.75/0.25	5700	7.0e15	2.4e16	4.6e6	1.27	7.9e-5
718 d	0.75/0.25	5700	7.0e15	2.4e16	2.4e6	1.27	7.9e-5
944 d	0.75/0.25	5700	7.0e15	2.4e16	6.9e5	1.27	7.9e-5

4.5 Summary

This chapter presents the results of a comprehensive study of SN 2007it for almost three years post-explosion. SN 2007it is a Type IIP supernova, most similar to SN 2004et, that shows some interesting characteristics and has produced $\sim$ 1.0 x $10^{-4} M_\odot$ of dust in its ejecta, likely in the cool dense shell created from CSM interaction. High late-time luminosities indicate that M_{Ni}= 0.09 $M_\odot$ was synthesized in the explosion, greater than seen in other SNe such as 1987A and 2004et. The [Ca II]/[O I] ratios post plateau are also much smaller than normally seen in a Type IIP, 0.70 prior to dust formation and 0.50 after. These two factors, a higher than normal Ni mass and a small [Ca II]/[O I], along with the expansion velocity of Hα at early times and of [O I] at later times suggest that SN 2007it may have had a progenitor mass $\geq 20 M_\odot$, which is quite large for a Type IIP SN. The late-time lightcurve and color evolution also suggests that a light echo exists around SN 2007it which will be discussed in detail in an upcoming paper. Estimates of oxygen mass suggest that 1.1-1.4 $M_\odot$ may be present, which is consistent with the Type II SNe 2004et and 1987A. The oxygen lines also show strange behavior not previously seen in a Type II SNe. The post-plateau spectra show a blueshifted component at -1300 km s^{-1} to the 6300 and 6364 Å lines, with no corresponding peak at +1300 km s^{-1}. This is likely due to emission from an asymmetric blob of O material ejected on the forward side of the SN during the explosion.

Modeling done on SN 2007it using our MOCCASIN radiative transfer code indicates that there was pre-existing dust surrounding the SN prior to explosion, and that up to $\sim$ 1.0 x $10^{-4} M_\odot$ formed in the ejecta after day 351. Up to 1 $M_\odot$ of dust would need to be produced per SN to account for the dust amounts seen at high-z according to the work of Todini & Ferrara (2001) and Nozawa et al. (2003). Recently, however, Cherchneff & Dwek (2010) have suggested that these models may overestimate these masses, which would be consistent with the values seen in nearby SNe. Even if the amount of dust produced in SN 2007it may not be large enough to account for the dust budget of early galaxies (Kozasa et al., 1989; Todini

& Ferrara, 2001), it is on par with other SNe such as 2007od (Andrews et al., 2010), 2004et Kotak et al. (2009), and SN 2006jc Mattila et al. (2008).

5. Conclusion

My thesis project was a study to detect, measure and model dust formation in nearby CCSNe. Surprisingly, dust mass estimates derived from the observed SEDs (spectral energy distributions) of the new targets presented in this thesis along with previously studied SNe, have been much lower than necessary to account for the dust observed in early-time galaxies. The sample of measured SNe is becoming significant but it appears that a typical CCSN is producing only 10^{-3}-10^{-4}M$_{\odot}$ of dust (see Table 5.1), well below the 1 M$_{\odot}$ needed to account for the large amounts of dust seen in the early Universe (Kozasa et al., 1989; Todini & Ferrara, 2001). SN 2004et has been found to have formed only a few times 10^{-3}M$_{\odot}$ of dust (Fabbri et al., 2011). Sugerman et al. (2006) showed that larger masses (10^{-2}M$_{\odot}$) of dust can be derived in the case of SN 2003gd if the dust is considered to be clumpy and mostly silicate, but Meikle et al. (2007) questioned these findings and derive smaller dust masses (10^{-4}M$_{\odot}$) for SN 2003gd. Finally, Ercolano et al. (2007), using similar methods to Sugerman et al. (2006), did not find that large amounts of dust had condensed in the Si-poor envelope of SN 1987A.

SN 2007od exhibits characteristics that have rarely been seen in a Type IIP SN. Optical V-band photometry reveals a very steep brightness decline between the plateau and nebular phases of $\sim$4.5 mag, likely due to SN 2007od containing only 6 x 10^{-3} M$_{\odot}$ of ^{56}Ni. The optical spectra show an evolution from normal Type IIP with broad Hα emission, to a complex, four component Hα emission profile exhibiting asymmetries caused by dust extinction after day 232. This is similar to the spectral evolution of the Type IIn SN 1998S, although no early-time narrow ($\sim$200 km s^{-1}) Hα component was present in SN 2007od. In both SNe, the intermediate-width Hα emission components are thought to arise in the interaction between the ejecta and its circumstellar medium (CSM). SN 2007od also shows a mid-infrared excess due to new dust. The evolution of the Hα profile and the presence of the mid-IR excess provide strong evidence that SN 2007od formed new dust before day 232. Late-time observations reveal a flattening of the visible light curve along with the exposure of a faint, broad Hα component similar to that seen pre-nebular phase. This is most likely due to the presence of a light echo, which accounts for the broad, underlying Hα component seen at late times. We believe the multi-peaked Hα emission is consistent with the interaction of the ejecta with a circumstellar ring or torus (for the inner components at $\pm$1500 km s^{-1}), and a single blob or cloud of circumstellar material out of the plane of the CSM ring (for the outer component at -5000 km s^{-1}). The most probable location for the formation of new dust is in the cool dense shell created by the interaction between the expanding ejecta and its CSM. Monte Carlo radiative transfer modeling of the dust emission from SN 2007od implies that up to $\sim$4 x 10^{-4}M$_{\odot}$ of new dust has formed. This is similar to the amounts of dust formed in other core-collapse supernovae such as SNe 1999em, 2004et, and 2006jc.

SN 2007it was one of the brightest CCSNe of 2007, with a peak V brightness of 13.1. The visible photometry shows a bright late-time luminosity, powered by the 0.09 M$_{\odot}$ of ^{56}Ni present in the ejecta. There is also a sudden drop in optical brightness after day 339, and a corresponding brightening in the IR due to new dust forming in the ejecta. CO and SiO emission, generally thought to be precursors to dust formation, may have been detected in the mid-IR photometry of SN 2007it. The optical spectra show stronger than average [O I] emission lines and weaker than average [Ca II] lines, which may indicate a 16 - 27 M$_{\odot}$ progenitor, on the higher end of expected Type IIP masses. Multi-component [O I] lines are also seen in the optical spectra, most likely caused by an asymmetric blob or a torus of

oxygen core material being ejected during the SN explosion. Interaction with circumstellar material prior to day 540 may have created a cool dense shell between the forward and reverse shocks where new dust is condensing. At late times there is also a flattening of the visible lightcurve as the ejecta luminosity fades and a surrounding light echo becomes visible. Radiative transfer models of SN 2007it SEDs indicate that up to 10^{-4} $M_{\odot}$ of new dust has formed in the ejecta, which is consistent with the amount of dust formed in other core collapse supernovae.

Table 5.1: CCSNe and their corresponding newly synthesized dust masses

SN	Type	Dust Mass ($M_{\odot}$)	References
1987A	II	7.5×10^{-4}	Ercolano et al. 2007
1998S	IIn	2×10^{-3}	Pozzo et al. 2004
1999em	IIP	$>10^{-4}$	Elmhamdi et al. 2003
2003gd	IIP	10^{-2}-10^{-4}	Sugerman et al. 2006, Meikle et al. 2004
2004et	IIP	1.5×10^{-3}	Fabbri et al. 2011
2004dj	IIP	8×10^{-4}	Szalai et al. 2010
2005af	IIP	4×10^{-4}	Kotak et al. 2008
2005ip	IIn	5×10^{-4}	Smith et al. 2008, Fox et al. 2009
2006jc	Ib	3×10^{-4}	Matilla et al. 2008
2007it	IIP	1×10^{-4}	Andrews et al. 2011
2007od	IIP	4×10^{-4}	Andrews et al. 2010

CCSNe occurring in the local universe may have different properties than those occurring in early galaxies. In particular, the first generation of (Population III) stars forming after galaxy formation will be very massive (100-200 $M_{\odot}$). Cherchneff & Dwek (2010) evaluate the dust masses produced in Population III high mass stars and find that based on the percentage of mixing of the elements in the ejecta and the specific compositions that a 170 $M_{\odot}$ progenitor could produce anywhere from 6-35 $M_{\odot}$ of dust while a 20 $M_{\odot}$ progenitor could be expected to produce 0.1 - 0.4 $M_{\odot}$. From these models, one would expect the more massive the progenitor the more massive the amount of synthesized dust, even in the nearby Universe. Unfortunately few progenitor masses have been estimated, with only a handful being resolved in high resolution HST images (for a full account see Smartt et al. (2009)) and others being surmised from various observables such as ^{56}Ni mass or the strengths of [O I] lines. Figure 5.1 shows a plot of progenitor mass versus newly synthesized dust mass. Very little can be inferred from the existing data but there is no discernible relationship between dust mass and progenitor mass.

This thesis work has added significant information to the very limited and sparse dataset on long-time contiunous observations of core collapse SNe. By following SNe 2007it and 2007od for over 1000 days in optical and infrared wavelengths I have found agreement with other studies that only small amounts of dust are being produced. I have also discovered that in these two objects, they both showed signs of circumstellar interaction at later times. This could imply that a high percentage, if not most, CCSNe will show some signs of CSM interaction if followed for long enough. The time at which the CSM interaction would become observable and the strength of the interaction would be highly dependent on the mass loss history of the progenitor, and the shock physics in the CSM surrounding the star prior to

explosion. SNe which explode very near the time of a major mass-loss event are likely to be classified as Type IIn, while others that have had more time elapsed since the last major mass loss, or those which only have a constant RSG wind mass loss will be classified as normal Type II which may or may not show CSM interaction at later times.

Understanding where and when SN/CSM interaction can occur is important to understanding the dust processing in all types of CCSNe. Interaction between the SN ejecta and the surrounding CSM can create both a forward and reverse shock. While the forward shock may be responsible for destroying some of the pre-existing dust, an area of cool, dense material can be created between the two shocks which has temperatures (< 1500 K) hospitable to grain formation. This can allow two areas of dust formation in a CCSNe, in the cool dense shell created from CSM interaction prior to day 300 and in the expanding SN ejecta after day 300. One must be careful to get observations of the SN at early times, specifically in the IR, to be able to detect this pre-existing CSM dust in order to rule out its contribution at later times when obtaining estimates for newly formed dust. I have found evidence of both types of dust formation in my thesis work, with SN 2007od forming dust in the CDS around day 200 and SN 2007it forming dust in the ejecta between day 350- 550.

This thesis has added significantly to the sparse full wavelength and time coverage observations of CCSNe, but there are other diagnostics which I would like to use in the upcoming years to add to the database of my work. For instance, mainly optical spectroscopy has been used for past observations, in the future I would also like to obtain near-IR spectroscopy in order to exploit the wavelength dependence of extinction to determine if the line asymmetry is caused by the presence of dust, or is actually intrinsic to the object. For instance comparing corresponding hydrogen emission lines Hα (6563 Å) with Paβ (1.28 μm) in Type II SNe, or comparing He I 5876 Å with either He I 1.08 μm or He I 2.06 μm in Type Ib or Ic SNe would help distinguish dust extinction from asymmetries in the SN explosion, for example. This type of comparison has not been used extensively in the past, and would be a powerful diagnostic tool. Also, the ejecta/CSM interaction, especially in Type IIn and Ib/c SNe, can be detectable for years after the SN explosion using the sensitivity of HST and large ground telescopes, as long as there is dense CSM available to run in to. For example the Type IIn SN 1986J is still quite bright (R= 20 mag), more than 20 years later (Millsajevic et al. 2008). Their late time brightnesses make them invaluable for observing transitions from SN to SN remnants. SNe are rarely observed after $\sim$100 days, so by revisiting these objects we may be able to still detect any residual dust emission and obtain a better understanding of late time dust-forming mechanisms. If there are light echoes present around these objects, using spectroscopy we may also be able to differentiate between echoes and new dust. Using HST it is even possible to visually resolve the echoes, which will provide strong constraints on the explosion geometries.

Although the sample is still small, this ever-growing body of evidence seems to indicate that low-mass CCSNe such as the ones seen today are likely not major contributors to dust in the early universe. None of them approach the $\sim$1 $M_{\odot}$ of dust per SN needed to account for the massive amounts of dust seen in early-time galaxies at high red-shift (Kozasa et al., 1989; Todini & Ferrara, 2001). Sloan et al. (2009) and Valiante et al. (2009) have both suggested that AGB stars can be more significant contributors to dust formation in early galaxies than once thought and Wesson et al. (2010) found that SN 2008S was likely a massive AGB star, not a supernova at all, which produced a significant amount of dust. SNe may then only play a small part in the dust formation in early galaxies. The sample is still very meager, and more such SNe need to be observed with good temporal and wavelength coverage to definitely answer the role of SNe as dust produces in high-z galaxies as well as the many open questions that still remain about the role of CCSNe to the dust budget galaxies. Specifically, is there a relationship between progenitor mass and dust mass, does redshift affect dust production

amounts or even compositions, and are CCSNe even needed to produce dust at high-z as originally thought, or can AGB stars and grain growth in the cool ISM produce the 10^8 $M_\odot$ detected? To help address these, more long-term multi-wavelength campaigns need to be taken, hopefully of objects with pre-explosion high-resolution imaging. With new SNe being discovered every day, the odds of existing high-quality images of the progenitor star increases. The continued attention to the disconnect between the amount of dust produced in nearby CCSNe to those when the Universe was less than 1 Gyr old may help answer important questions as to the role of CCSNe in the dust budget of the Universe.

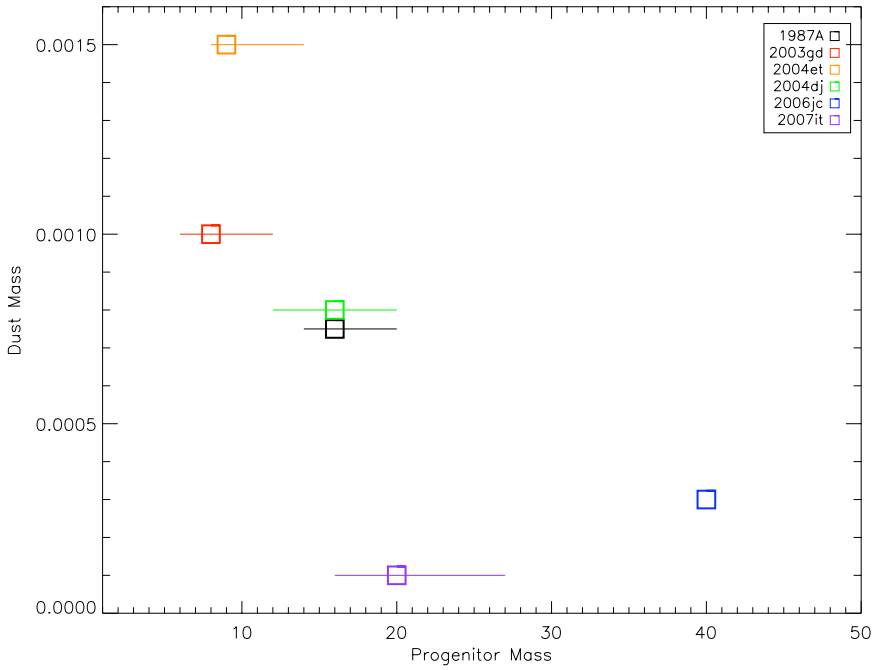

Figure 5.1: Plot of progenitor mass versus dust mass of the few CCSNe with measured progenitor masses. Dust masses are from references listed in Table 5.1, and progenitor masses are from Smartt et al. (2009) and Andrews et al. (2011).

Bibliography

Andrews, J. E., et al. 2010, ApJ, 715, 541

—. 2011, ApJ, 731, 47

Anupama, G. C., Sahu, D. K., Gurugubelli, U. K., Prabhu, T. P., Tominaga, N., Tanaka, M., & Nomoto, K. 2009, MNRAS, 392, 894

Bertoldi, F., Carilli, C. L., Cox, P., Fan, X., Strauss, M. A., Beelen, A., Omont, A., & Zylka, R. 2003, A&A, 406, L55

Bianchi, S., & Schneider, R. 2007, MNRAS, 378, 973

Blondin, S., & Calkins, M. 2007, Central Bureau Electronic Telegrams, 1119, 1

Bouchet, P., & Danziger, I. J. 1993, A&A, 273, 451

Bouchet, P., Slezak, E., Le Bertre, T., Moneti, A., & Manfroid, J. 1989, A&AS, 80, 379

Caldwell, J. A. R., et al. 1993, MNRAS, 262, 313

Cherchneff, I., & Dwek, E. 2010, ApJ, 713, 1

Chevalier, R. A., & Fransson, C. 1994, ApJ, 420, 268

Chevalier, R. A., Fransson, C., & Nymark, T. K. 2006, ApJ, 641, 1029

Chugai, N. N. 1988a, APSS, 146, 375

—. 1988b, Soviet Astronomy Letters, 14, 334

Contreras, C., Morrell, N., Gonzalez, S., & Lee, K. 2007, Central Bureau Electronic Telegrams, 1068, 1

Couderc, P. 1939, Annales d'Astrophysique, 2, 271

DePoy, D. L., et al. 2003, in Society of Photo-Optical Instrumentation Engineers (SPIE) Conference Series, Vol. 4841, Society of Photo-Optical Instrumentation Engineers (SPIE) Conference Series, ed. M. Iye & A. F. M. Moorwood, 827–838

Dessart, L., Livne, E., & Waldman, R. 2010, ArXiv e-prints

Draine, B. T. 2009, in Astronomical Society of the Pacific Conference Series, Vol. 414, Astronomical Society of the Pacific Conference Series, ed. T. Henning, E. Grün, & J. Steinacker, 453–+

Draine, B. T., & Lee, H. M. 1984, ApJ, 285, 89

Dwek, E. 1985, ApJ, 297, 719

—. 1998, ApJ, 501, 643

Dwek, E., & Cherchneff, I. 2010, ArXiv e-prints

Dwek, E., Galliano, F., & Jones, A. P. 2007, ApJ, 662, 927

Eldridge, J. J., & Tout, C. A. 2004, MNRAS, 353, 87

Elmhamdi, A., Chugai, N. N., & Danziger, I. J. 2003a, A&A, 404, 1077

Elmhamdi, A., Danziger, I. J., Cappellaro, E., Della Valle, M., Gouiffes, C., Phillips, M. M., & Turatto, M. 2004, A&A, 426, 963

Elmhamdi, A., et al. 2003b, MNRAS, 338, 939

Emmering, R. T., & Chevalier, R. A. 1989, ApJ, 338, 388

Ercolano, B., Barlow, M. J., & Storey, P. J. 2005, MNRAS, 362, 1038

Ercolano, B., Barlow, M. J., & Sugerman, B. E. K. 2007, MNRAS, 375, 753

Evans, R. O., Nitschki, D., & Quirk, S. 2007, Central Bureau Electronic Telegrams, 1065, 1

Fazio, G. G., et al. 2004, ApJS, 154, 10

Filippenko, A. V. 1997, ARA&A, 35, 309

Fox, O., et al. 2009, ApJ, 691, 650

Fox, O. D., Chevalier, R. A., Dwek, E., Skrutskie, M. F., Sugerman, B. E. K., & Leisenring, J. M. 2010, ArXiv e-prints

Fransson, C., & Chevalier, R. A. 1987, ApJL, 322, L15

—. 1989, ApJ, 343, 323

Fransson, C., et al. 2005, ApJ, 622, 991

Fukugita, M., Ichikawa, T., Gunn, J. E., Doi, M., Shimasaku, K., & Schneider, D. P. 1996, AJ, 111, 1748

Gehrz, R. 1989, in IAU Symposium, Vol. 135, Interstellar Dust, ed. L. J. Allamandola & A. G. G. M. Tielens, 445–+

Gerardy, C. L., Fesen, R. A., Höflich, P., & Wheeler, J. C. 2000, AJ, 119, 2968

Grassberg, E. K., Imshennik, V. S., & Nadyozhin, D. K. 1971, APSS, 10, 28

Hamuy, M. 2003, ApJ, 582, 905

Hanner, M. 1988, Grain optical properties, Tech. rep.

Heger, A., Fryer, C. L., Woosley, S. E., Langer, N., & Hartmann, D. H. 2003, ApJ, 591, 288

Hendry, M. A., et al. 2005, MNRAS, 359, 906

Holtzman, J. A., Burrows, C. J., Casertano, S., Hester, J. J., Trauger, J. T., Watson, A. M., & Worthey, G. 1995, PASP, 107, 1065

Hook, I. M., Jørgensen, I., Allington-Smith, J. R., Davies, R. L., Metcalfe, N., Murowinski, R. G., & Crampton, D. 2004, PASP, 116, 425

Immler, S., & Brown, P. J. 2007, The Astronomer's Telegram, 1259, 1

Immler, S., Brown, P. J., Filippenko, A. V., & Pooley, D. 2007a, The Astronomer's Telegram, 1290, 1

Immler, S., Pooley, D., Brown, P. J., Li, W., & Filippenko, A. V. 2007b, The Astronomer's Telegram, 1284, 1

Itagaki, K., et al. 2007, IAUC, 8874, 3

Jeffery, D. J., & Branch, D. 1990, in Supernovae, Jerusalem Winter School for Theoretical Physics, ed. J. C. Wheeler, T. Piran, & S. Weinberg, 149

Kasen, D., & Woosley, S. E. 2009, ApJ, 703, 2205

Kawabata, K. S., Tanaka, M., Maeda, K., Hattori, T., Nomoto, K., Tominaga, N., & Yamanaka, M. 2009, ApJ, 697, 747

Kiewe, M., et al. 2010, ArXiv e-prints

Kotak, R., Meikle, P., van Dyk, S. D., Höflich, P. A., & Mattila, S. 2005, ApJL, 628, L123

Kotak, R., et al. 2006, APJL, 651, L117

—. 2009, ApJ, 704, 306

Kozasa, T., Hasegawa, H., & Nomoto, K. 1989, ApJ, 344, 325

—. 1991, A&A, 249, 474

Landolt, A. U. 2009, AJ, 137, 4186

Leonard, D. C., Filippenko, A. V., Barth, A. J., & Matheson, T. 2000, ApJ, 536, 239

Lucy, L. B., Danziger, I. J., Gouiffes, C., & Bouchet, P. 1989, in Lecture Notes in Physics, Berlin Springer Verlag, Vol. 350, IAU Colloq. 120: Structure and Dynamics of the Interstellar Medium, ed. G. Tenorio-Tagle, M. Moles, & J. Melnick, 164–+

Maeda, K., Taubenberger, S., Sollerman, J., Mazzali, P. A., Leloudas, G., Nomoto, K., & Motohara, K. 2010, ApJ, 708, 1703

Maeda, K., et al. 2007, ApJL, 658, L5

Maguire, K., et al. 2010, MNRAS, 284

Makovoz, D., & Marleau, F. R. 2005, PASP, 117, 1113

Mathis, J. S., Rumpl, W., & Nordsieck, K. H. 1977, ApJ, 217, 425

Mattila, S., et al. 2008, MNRAS, 389, 141

Meikle, W. P. S., et al. 2006, ApJ, 649, 332

—. 2007, ApJ, 665, 608

Michałowski, M. J., Murphy, E. J., Hjorth, J., Watson, D., Gall, C., & Dunlop, J. S. 2010a, A&A, 522, A15+

Michałowski, M. J., Watson, D., & Hjorth, J. 2010b, ApJ, 712, 942

Mikuz, H., & Maticic, S. 2007, Central Bureau Electronic Telegrams, 1116, 1

Milisavljevic, D., Fesen, R. A., Gerardy, C. L., Kirshner, R. P., & Challis, P. 2010, ApJ, 709, 1343

Miller, A. A., Smith, N., Li, W., Bloom, J. S., Chornock, R., Filippenko, A. V., & Prochaska, J. X. 2010, AJ, 139, 2218

Miller, A. A., et al. 2009, ApJ, 690, 1303

Misra, K., Pooley, D., Chandra, P., Bhattacharya, D., Ray, A. K., Sagar, R., & Lewin, W. H. G. 2007, MNRAS, 381, 280

Modjaz, M., Kirshner, R. P., Blondin, S., Challis, P., & Matheson, T. 2008, ApJL, 687, L9

Morgan, H. L., & Edmunds, M. G. 2003, MNRAS, 343, 427

Nozawa, T., Kozasa, T., Umeda, H., Maeda, K., & Nomoto, K. 2003, ApJ, 598, 785

Pastorello, A., et al. 2004, MNRAS, 347, 74

—. 2005, MNRAS, 360, 950

—. 2009, MNRAS, 394, 2266

Patat, F. 2005, MNRAS, 357, 1161

Patat, F., Benetti, S., Cappellaro, E., & Turatto, M. 2006, MNRAS, 369, 1949

Pinto, P. A., Woosley, S. E., & Ensman, L. M. 1988, ApJL, 331, L101

Pojmanski, G. 2007, IAUC, 8875, 1

Pooley, D., et al. 2002, ApJ, 572, 932

Pozzo, M., Meikle, W. P. S., Fassia, A., Geballe, T., Lundqvist, P., Chugai, N. N., & Sollerman, J. 2004, MNRAS, 352, 457

Pronik, V. I., Chuvaev, K. K., & Chugai, N. N. 1976, Soviet Astronomy Letters, 20, 666

Pun, C. S. J., et al. 1995, APJS, 99, 223

Roche, P. F., Aitken, D. K., & Smith, C. H. 1991, MNRAS, 252, 39P

Sahu, D. K., Anupama, G. C., Srividya, S., & Muneer, S. 2006, MNRAS, 372, 1315

Shaw, B., K., Q., & M.E., K. 2009, Baltimore: STScI, Version 7.0

Sirianni, M., et al. 2005, PASP, 117, 1049

Sloan, G. C., et al. 2009, Science, 323, 353

Smartt, S. J., Eldridge, J. J., Crockett, R. M., & Maund, J. R. 2009, MNRAS, 395, 1409

Smith, N., Foley, R. J., & Filippenko, A. V. 2008, ApJ, 680, 568

Sollerman, J., Cumming, R. J., & Lundqvist, P. 1998, ApJ, 493, 933

Stritzinger, M., et al. 2009, ApJ, 696, 713

Sugerman, B. E. K. 2003, AJ, 126, 1939

—. 2005, ApJL, 632, L17

Sugerman, B. E. K., et al. 2006, Science, 313, 196

Suntzeff, N. B., Phillips, M. M., Depoy, D. L., Elias, J. H., & Walker, A. R. 1991, AJ, 102, 1118

Taubenberger, S., et al. 2009, MNRAS, 397, 677

Todini, P., & Ferrara, A. 2001, MNRAS, 325, 726

Tully, R. B. 1988, Nearby galaxies catalog, ed. Tully, R. B.

Tully, R. B., Shaya, E. J., Karachentsev, I. D., Courtois, H. M., Kocevski, D. D., Rizzi, L., & Peel, A. 2008, ApJ, 676, 184

Turatto, M., Cappellaro, E., Benetti, S., & Danziger, I. J. 1993a, MNRAS, 265, 471

Turatto, M., Cappellaro, E., Danziger, I. J., Benetti, S., Gouiffes, C., & della Valle, M. 1993b, MNRAS, 262, 128

Uomoto, A. 1986, ApJL, 310, L35

Valiante, R., Schneider, R., Bianchi, S., & Andersen, A. C. 2009, MNRAS, 397, 1661

Vinkó, J., et al. 2006, MNRAS, 369, 1780

Weaver, T. A., & Woosley, S. E. 1980, in Annals of the New York Academy of Sciences, Vol. 336, Ninth Texas Symposium on Relativistic Astrophysics, ed. J. Ehlers, J. J. Perry, & M. Walker, 335–357

Welch, D. L., Clayton, G. C., Campbell, A., Barlow, M. J., Sugerman, B. E. K., Meixner, M., & Bank, S. H. R. 2007, ApJ, 669, 525

Wesson, R., et al. 2010, MNRAS, 403, 474

Winkler, P. F., & Kirshner, R. P. 1985, ApJ, 299, 981

Witt, A. N., & Gordon, K. D. 1996, ApJ, 463, 681

Wooden, D. H., Rank, D. M., Bregman, J. D., Witteborn, F. C., Tielens, A. G. G. M., Cohen, M., Pinto, P. A., & Axelrod, T. S. 1993, APJS, 88, 477

Woosley, S. E., Pinto, P. A., Martin, P. G., & Weaver, T. A. 1987, ApJ, 318, 664

Woosley, S. E., & Weaver, T. A. 1986, A&A, 24, 205

Zhang, T., Wang, X., Li, W., Zhou, X., Ma, J., Jiang, Z., & Chen, J. 2006, AJ, 131, 2245

Appendix A: Photometric Standards

The photometric sequences of tertiary standard stars used for both SMARTS and Gemini photometry were obtained using the Y4KCam CCD on the Yale 1.0m telescope operated at the Cerro Tololo Inter-American Observatory on the nights of 2008 October 28 and 2009 February 27. The Y4KCam offered a field of view of $\sim 20'$x$20'$ and employed a set of standard Johnson-Kron-Cousins broadband BVRI filters. The processing of all images to remove instrumental signatures was accomplished using the standard techniques of subtracting a median filtered bias frame and dividing by master twilight flat field images for each filter. Also, the fringing effects in the I-band exposures were removed by scaling and subtracting a master fringe frame from the program images. In order to transform the instrumental magnitudes to the standard system, we observed between 30 and 35 different stars (depending on filter) from the lists of Landolt (2009) in addition to the SN fields. Importantly, these stars were selected due to their ample range in color, and they were observed both near zenith and at a high airmass ($\sim$1.75). Thus, they provided a viable sample of stars from which to derive accurate color and extinction coeffecients as well as magnitude zero-points for each filter. The resulting RMS scatter of the residuals from the transformations revealed that the photometry for selected stars in the fields derived from the observations is accurate on the 1-2% level depending on filter.

Table 5.2: Tertiary BVRI Standards for NGC 5530

Star	B	V	R	I
A	17.743 ± 0.012	17.060 ± 0.001	16.655 ± 0.012	16.272 ± 0.017
B	19.115 ± 0.039	17.667 ± 0.011	16.696 ± 0.015	15.648 ± 0.013
C	19.235 ± 0.040	18.099 ± 0.015	17.485 ± 0.014	16.945 ± 0.025
D	18.057 ± 0.014	17.254 ± 0.021	16.772 ± 0.033	16.209 ± 0.088
E	18.652 ± 0.029	17.219 ± 0.016	16.240 ± 0.007	15.154 ± 0.011
F	17.672 ± 0.012	16.818 ± 0.009	16.318 ± 0.008	15.812 ± 0.014
G	18.281 ± 0.017	17.587 ± 0.033	17.205 ± 0.020	16.778 ± 0.028

Table 5.3: Tertiary BVRI Standards for UGC 12846

Star	B	V	R	I
A	16.989 ± 0.014	15.938 ± 0.011	15.338 ± 0.006	14.820 ± 0.017
B	17.480 ± 0.020	16.357 ± 0.011	15.720 ± 0.006	15.153 ± 0.018
C	17.266 ± 0.015	16.109 ± 0.011	15.403 ± 0.006	14.786 ± 0.017
D	17.966 ± 0.019	17.133 ± 0.014	16.672 ± 0.010	16.343 ± 0.068
E	18.146 ± 0.021	17.240 ± 0.014	16.708 ± 0.010	16.267 ± 0.039

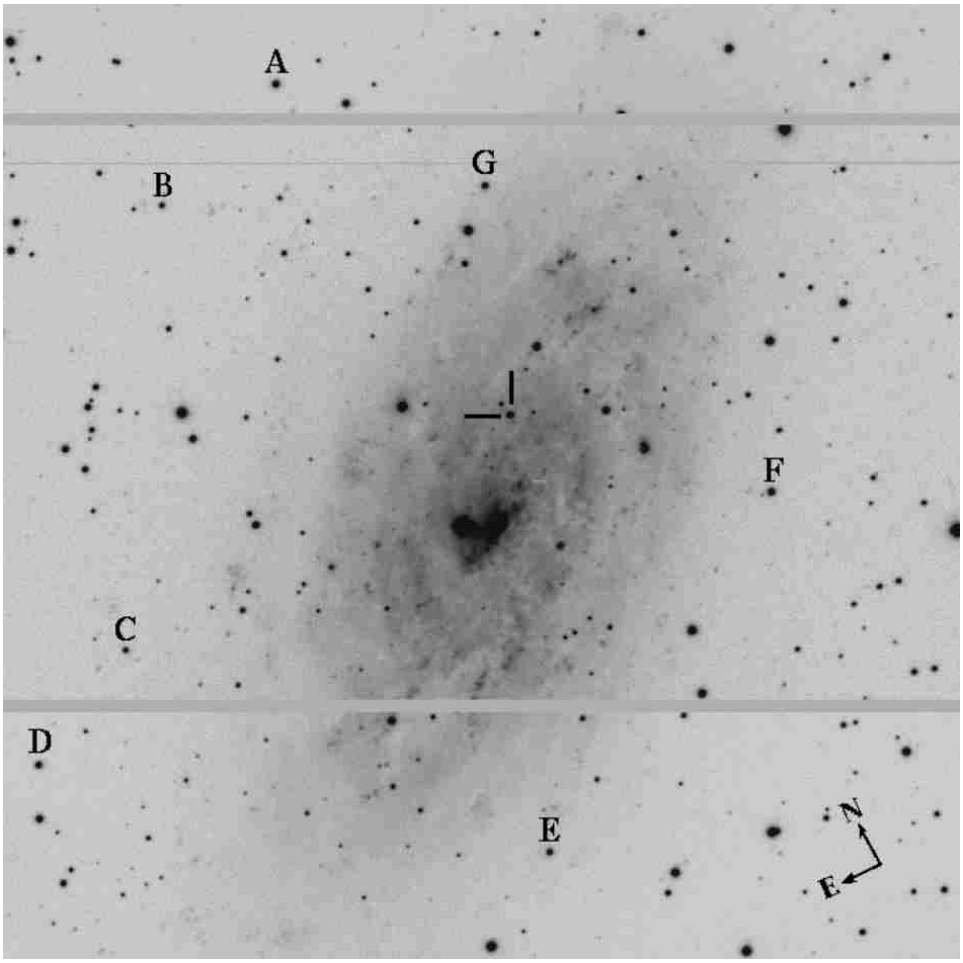

Figure 5.2: Image of NGC 5530 taken in the g′ band with Gemini South on 2008 April 12. The tertiary standards listed in Table 5.2 are labeled alphabetically, and the SN is indicated at the center of the image. The image is 4″.2 x 4″.2.

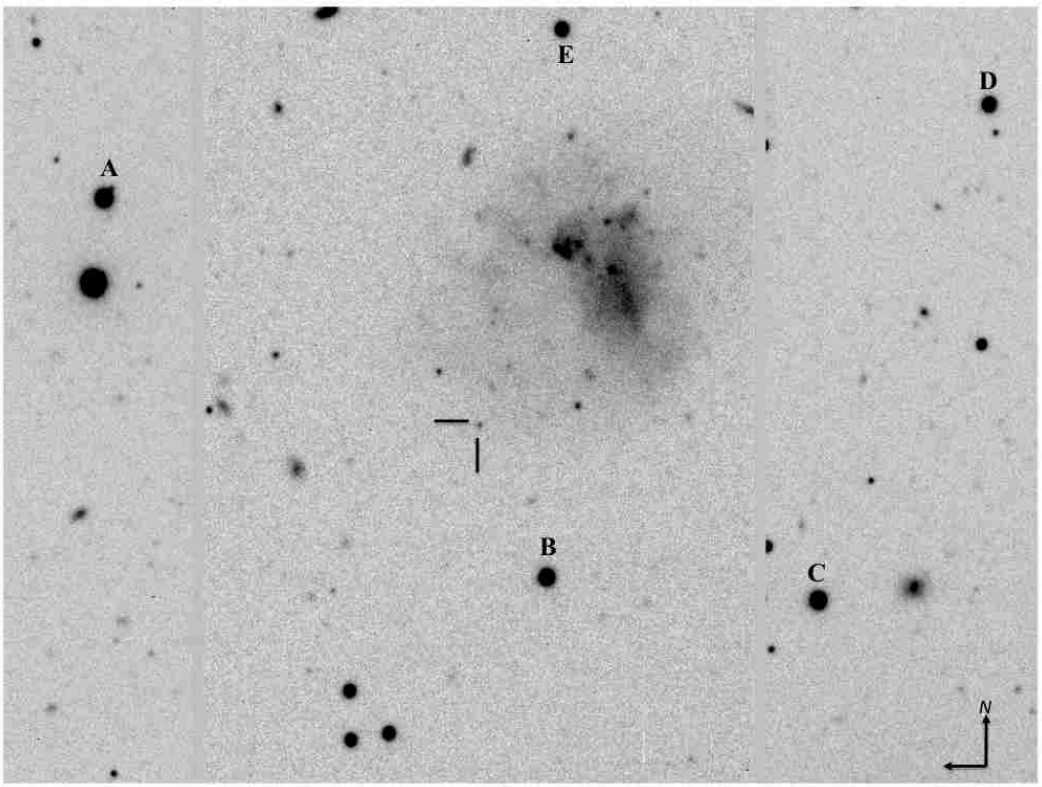

Figure 5.3: The field of SN 2007od showing the location of the tertiary standards (designated alphabetically) listed in Table5.3. The location of SN 2007od is marked. North is up and east is left. The image is 4″.7 x 3″.1 and was taken with Gemini/GMOS-S on 2008 August 29 with the g′ filter.

Table 5.4: Tertiary BVRI Standards for NGC 7418A

Star	B	V	R	I
A	16.601 ± 0.014	15.987 ± 0.011	15.598 ± 0.008	15.247 ± 0.017
B	16.093 ± 0.014	15.524 ± 0.011	15.140 ± 0.005	14.758 ± 0.017
C	16.326 ± 0.014	15.471 ± 0.011	14.965 ± 0.005	14.481 ± 0.017
D	16.663 ± 0.015	15.770 ± 0.011	15.246 ± 0.005	14.821 ± 0.017

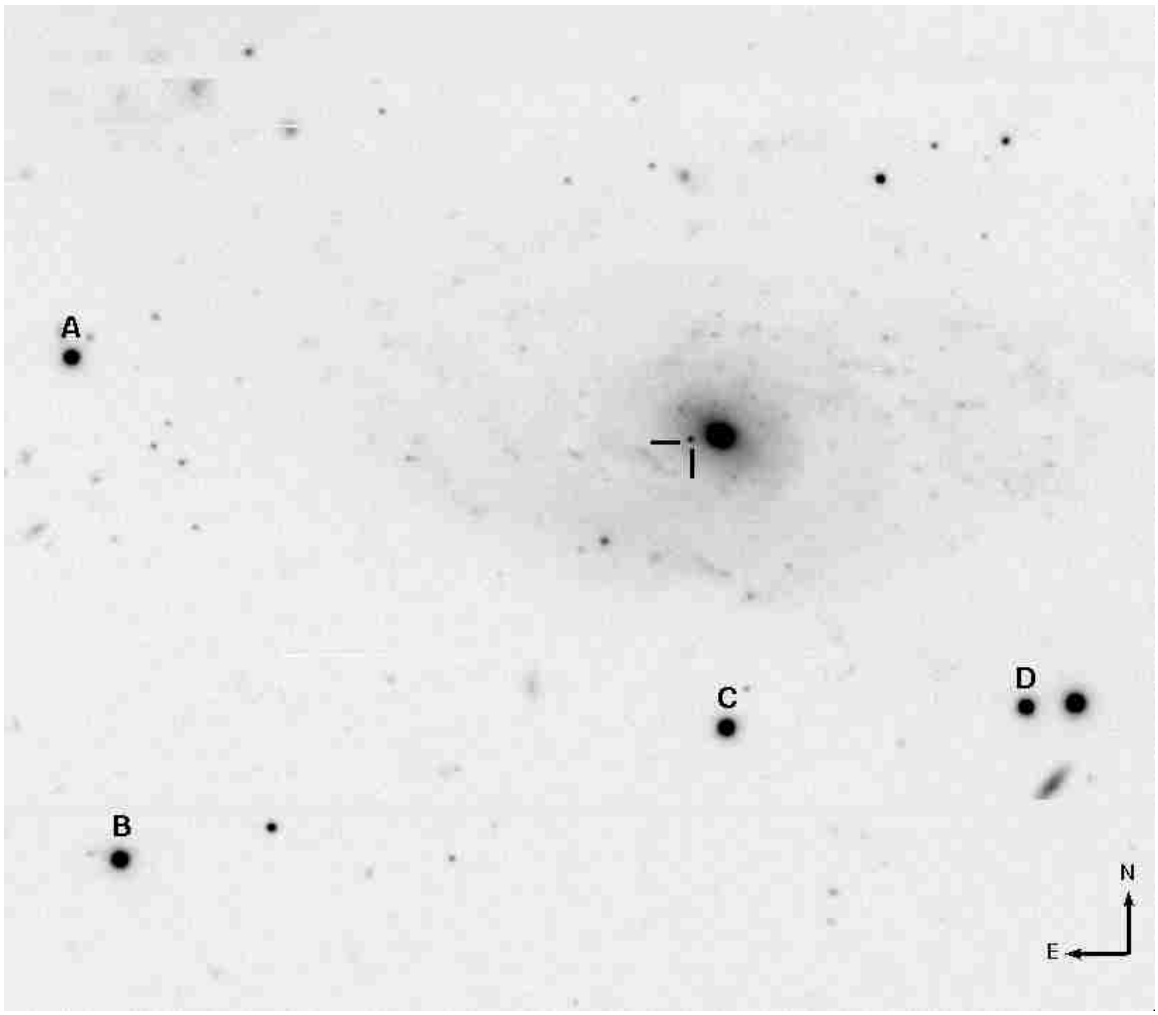

Figure 5.4: The field of SN 2007oc showing the location of the tertiary standards (designated alphabetically) listed in Table 5.4. The location of SN 2007oc is marked. North is up and east is left. The image is 3″.5 x 4″.0 and was taken with Gemini/GMOS-S on 2008 June 12 with the g′ filter.

Appendix B: Permission to Reproduce Copyrighted Material

The following is reproduced from the Institute of Physics website, which allows me the right to reproduce the materials in Chapters 3 and 4, for which I am the author and for which the manuscripts have been cited in the text:

Before your article can be published in an American Astronomical Society (AAS) journal, we require you to grant and assign the entire copyright in it to the AAS. The copyright consists of all rights protected by the copyright laws of the United States and of all foreign countries, in all languages and forms of communication, including the right to furnish the article or the abstracts to abstracting and indexing services, and the right to republish the entire article in any format or medium. In return, the AAS grants to you the non-exclusive right of republication, subject only to your giving appropriate credit to the journal in which your article is published. This non-exclusive right of republication includes your right to allow reproduction of parts of your article wherever you wish, and permits you to post the published (PDF) version of your article on your personal web site. To protect the copyright in your article, the original copyright notice as it appears in the journal should be included in the credit. http://iopscience.iop.org/0004-637X/page/Copyright+and+permissions

Vita

Jennifer Erin Andrews was born March 10, 1983 to David and Wanda Andrews in Florence, South Carolina. She attended South Florence High School where she graduated salutatorian, and went on to receive her Bachelor of Science degree in Physics from the College of Charleston, in Charleston, South Carolina, in May 2005. During the summer of 2004 she worked at Maria Mitchell Observatory in Nantucket, Massachusetts where she met Dr. Geoffrey Clayton who would become her future thesis advisor. After a year working for the start-up science outreach organization ScienceSouth in Florence, South Carolina, she left the inflatable planetarium behind and began graduate school in Physics at Louisiana State University in the Fall of 2006 where she studied not only dust in supernovae but also practical string theory. She is currently a doctoral student expecting graduation in May 2011.